Icarus 270 (2016) 41–56

Contents lists available at ScienceDirect

Icarus

journal homepage: www.journals.elsevier.com/icarus

Structure of Titan's evaporites

D. Cordier [a,b,*], T. Cornet [c], J.W. Barnes [d], S.M. MacKenzie [d], T. Le Bahers [e], D. Nna-Mvondo [f], P. Rannou [a], A.G. Ferreira [g]

[a] Groupe de Spectrométrie Moléculaire et Atmosphérique, UMR 6089 Campus Moulin de la Housse, BP 1039, Université de Reims Champagne-Ardenne, 51687 Reims, France
[b] Université de Franche-Comté, Institut UTINAM, CNRS/INSU, UMR 6213, 25030 Besançon Cedex, France
[c] European Space Agency (ESA), European Space Astronomy Centre (ESAC), P.O. BOX 78, E-28691 Villanueva de la Cañada (Madrid), Spain
[d] Department of Physics, University of Idaho, Engineering-Physics Building, Moscow, ID 83844, USA
[e] Université de Lyon, Université Claude Bernard Lyon 1, ENS Lyon, Laboratoire de Chimie UMR5182, 46 allée d'Italie, 69007 Lyon Cedex 07, France
[f] Laboratoire de Planétologie et Géodynamique LPGNantes, UMR CNRS 6112, 2, rue de la Houssinière, BP 92208, 44322 Nantes Cedex 3, France
[g] Departamento de Engenharia Quimica, Universidade de Coimbra, Coimbra 3030-290, Portugal

ARTICLE INFO

Article history:
Received 31 March 2015
Revised 2 December 2015
Accepted 22 December 2015
Available online 31 December 2015

Keywords:
Satellites, surfaces
Saturn, satellites
Titan, surface

ABSTRACT

Numerous geological features that could be evaporitic in origin have been identified on the surface of Titan. Although they seem to be water–ice poor, their main properties – chemical composition, thickness, stratification – are essentially unknown. In this paper, which follows on a previous one focusing on the surface composition (Cordier, D., Barnes, J.W., Ferreira, A.G. [2013b]. Icarus 226(2),1431–1437), we provide some answers to these questions derived from a new model. This model, based on the up-to-date thermodynamic theory known as "PC-SAFT", has been validated with available laboratory measurements and specifically developed for our purpose. 1-D models confirm the possibility of an acetylene and/or butane enriched central layer of evaporitic deposit. The estimated thickness of this acetylene–butane layer could explain the strong RADAR brightness of the evaporites. The 2-D computations indicate an accumulation of poorly soluble species at the deposit's margin. Among these species, HCN or aerosols similar to tholins could play a dominant role. Our model predicts the existence of chemically trimodal "bathtub rings" which is consistent with what it is observed at the south polar lake Ontario Lacus. This work also provides plausible explanations to the lack of evaporites in the south polar region and to the high radar reflectivity of dry lakebeds.

1. Introduction

Among many other fascinating features, Titan, the largest satellite of Saturn, hosts lakes and seas (Stofan et al., 2007) likely filled by liquid hydrocarbons containing some amount of dissolved atmospheric nitrogen and various organic compounds (Dubouloz et al., 1989; Cordier et al., 2009, 2013a).

In Cordier et al. (2013b) (hereafter PAP1), the authors only derived a chemical composition for the external surface of Titan's putative evaporites. Butane and acetylene were found to be the most likely main components of these external layers, but this result has several restrictions, the most obvious being the lack of information concerning the spatial structure of the evaporitic deposits. Indeed, in PAP1, neither vertical stratification nor horizontal variations of composition were considered; consequently the model can be labeled "0-D". The 1-D or 2-D models of evaporitic deposition are of interest as the subsequent structure is potentially observable at the margins of these geological units. Moreover, a future lander could drill into these layers and perform detailed analysis or a Titan boat could directly measure dissolved solids with a mass spectrometer (Stofan et al., 2011).

In a laboratory study, Malaska et al. (2012) obtained interesting and illustrative result on the evaporitic crystallization process with exotic materials. After full evaporation of their working fluid (heptane at room temperature in replacement of methane and/or ethane in cryogenic conditions), a "playa" composed of the sequence of the four organic compounds initially dissolved in the

Abbreviations: PC-SAFT, Perturbed-Chain Statistical Associating Fluid Theory; VIMS, Visual and Infrared Mapping Spectrometer; RST, Regular Solution Theory; EoS, equation of state; VLE, vapor–liquid equilibrium; SLE, solid–liquid equilibrium; NIST, National Institute of Standards and Technology; DST, density functional theory; GCM, Global Circulation Model.

* Corresponding author at: Groupe de Spectrométrie Moléculaire et Atmosphérique, UMR 6089 Campus Moulin de la Housse, BP 1039, Université de Reims Champagne-Ardenne, 51687 Reims, France.
E-mail address: daniel.cordier@univ-reims.fr (D. Cordier).

http://dx.doi.org/10.1016/j.icarus.2015.12.034
0019-1035/

liquid was left behind. It should be noticed that some species used as analogs in this experimental approach do not follow the expected behavior based on their respective solubilities. This could be explained by the specific conditions of the laboratory simulation. Already in both VIMS[1] and RADAR data, chemical composition gradients appear to surround lakebeds (Barnes et al., 2009, 2011). Barnes et al. (2009) observed several separate *annuli* following the contour of the partially evaporated lake Ontario Lacus at Titan's south pole. Moriconi et al. (2010) tentatively detected organics and nitriles in a ramp along the shore of the same lake, suggesting that sediments and evaporites could coexist around this object. A model of evaporite layer structure may also shed light on the possible cause of the relatively high RADAR reflectivity observed in dry lakebeds. Indeed, as noticed by Barnes et al. (2011), this high reflectivity remains unexplained and could be caused by volume scattering if the evaporite layer is at least several centimeter thick or contains subsurface horizons (see also Section 3.3).

As a first step in PAP1, the Regular Solution Theory (hereafter RST) was employed to mimic the non-ideal effect in cryogenic solutions. Unfortunately, this approach is clearly limited (Cordier et al., 2012). Thus, the model of dissolution has been substantially improved in this work by the use of the Perturbed-Chain Statistical Associating Fluid Theory (hereafter PC-SAFT) equation of state (Gross and Sadowski, 2001) which is widely employed in the chemical engineering community. The PC-SAFT has been successfully introduced to the study of Titan by Tan et al. (2013, 2015) and Luspay-Kuti et al. (2015). Another improvement on the RST approach from PAP1 is the derivation of molar volumes of the relevant molecular solids from the properties of their crystal structure. The influence of the pressure on these volumes is moreover studied using state of the art quantum chemical calculations. We emphasize that the Modified Van Laar (MLV) model developed by Glein and Shock (2013) belongs to the RST family and relies, as does our model, on parameters regressed on empirical data. For the only solid organic considered by Glein and Shock (2013), *i.e.* acetylene, we have used the same experimental measurements, namely those published by Neumann and Mann (1969).

Our paper is organized as follows. In Section 2, we describe our new PC-SAFT based model, and we give details concerning the properties of the different molecular solids involved. We also specify the atmospheric model taken into consideration. Section 3 is devoted to results obtained with our 1-D model: for a given initial state (*i.e.* depth of liquid, assumed composition of solutes and solvents) a possible vertical structure is proposed. The question of the maximum thickness of evaporite deposited is also addressed. Adopting a plausible topography, in Section 4 we compute what could be the species segregation across a lakebed shore. Finally, we discuss our results and conclude in Sections 5 and 6.

2. The model of solutes properties

Although other possible sources are available in the literature, we have chosen to keep the list of studied solutes from the work of Lavvas et al. (2008a,b). This has the advantage of facilitating the comparisons with previous work (PAP1) and limits the potential sources of uncertainties which are inevitably multiplied by introducing more species. However, in the last section of the paper we will discuss the occurrence and the possible role of the compounds not included in our "standard" mixture. Although theoretical models (Lavvas et al., 2008a,b) argue in favor of their presence, we are aware that acetylene has not yet been firmly detected at the surface (Clark et al., 2010; Moriconi et al., 2010) and that butane has not been observed in the atmosphere.

Beside the solvents, considered as a ternary mixture of N_2, CH_4 and C_2H_6, we therefore consider a set of six species, listed in Table 1, which are assumed to be deposited to the surface of Titan or extracted from the "soil" by cryogenic solvents (after being previously produced in the atmosphere). In photochemical models (Lavvas et al., 2008a,b), they reach their temperature of solidification; therefore it can be hypothesized that they form exotic organic snows. Once they fall to the surface of Titan, these six species (*i.e.* HCN, C_4H_{10}, C_2H_2, CH_3CN, CO_2, C_6H_6) either remain in the solid state due to local conditions or will be dissolved in cryogenic solvents. Species that have been detected by observations or produced in photochemical models but are never found at temperatures below their freezing point are not considered as potential lake solutes – this is the case for ethylene. The microphysics of the formation of organic snows is ignored, although it could be the subject of interesting research in the future.

In the next section, we describe the adopted solubility theory and the method employed to get reliable molar volumes for organic solids.

2.1. The model of solubility

Similar to what has been done in PAP1, our solubility estimations are made by solving the equation

$$\ln \Gamma_i X_{i,sat} = -\frac{\Delta H_{i,m}}{RT_{i,m}}\left(\frac{T_{i,m}}{T} - 1\right) \quad (1)$$

where $X_{i,sat}$ is the mole fraction of the compound i at saturation and Γ_i is the activity coefficient of the considered species. $T_{i,m}$ and $\Delta H_{i,m}$ are melting temperature and enthalpy of melting respectively. The temperature of the system is denoted T, and R is the gas constant. This relation can be found, for instance, in the textbook by Poling et al. (2007). The physical meaning of Eq. (1) is that a thermodynamic equilibrium between the considered precipitated solid i and the liquid solution – Eq. (1) is nothing more than an equality of chemical potential. We emphasize that $X_i < X_{i,sat}$ can easily occur for a stable state, while situations where $X_i > X_{i,sat}$ are metastable. Commonly, metastable states are not sustainable: any perturbation ignites crystallization and the corresponding mole fractions are adjusted such as $X_i = X_{i,sat}$. The overabundance of species i is deposited at the bottom of the system. In PAP1 and in Glein and Shock (2013), the limitation of the validity of Eq. (1) is mentioned, an in depth discussion of that aspect will be put forward in the appendix of this paper. Cordier et al. (2012) have shown the flaws of the RST, as have other authors (Glein and Shock, 2013). At its core, the RST is a generalization of a model established for binary mixtures. The main caveat concerning the RST probably lies in its weak physical foundation. In contrast, the equation of state (EoS) called PC-SAFT[2] Gross and Sadowski (2001), which belongs to the vast family of the SAFT EoS, is molecular based. Indeed, PC-SAFT is derived, contrary to the RST, from the statistical physics. Each type of molecule is represented by parameters related to its individual microscopic properties. In that sense, PC-SAFT can be considered more profound than theories belonging to the RST family. Furthermore, PC-SAFT has proved to be one of the most powerful types of EoS for the liquid and vapor states. This theory is the subject of numerous works in the field of thermophysics. Here, the activity coefficient Γ_i that appears in Eq. (1) will be computed with the help of PC-SAFT. For this application to solid–liquid equilibrium (SLE), the activity coefficient is written as the ratio $\Gamma_i = \Phi_i^L/\Phi_i^{L0}$, where Φ_i^L is the fugacity coefficient of the species i and Φ_i^{L0} is the fugacity coefficient of the pure subcooled liquid of the same compound. In the frame of PC-SAFT, molecules are considered as "chains" of segments where each molecule is

[1] Visual and Infrared Mapping Spectrometer.

[2] Perturbed-Chain Statistical Associating Fluid Theory.

Table 1
Solids assumed to be dissolved in the lake and some of their properties.

Species	Precipitation rate molecules ($cm^{-2}\,s^{-1}$)	Melting temperature (K)	Enthalpy melting ($kJ\,mol^{-1}$)
HCN	1.3×10^{8}[a]	260.0	8.406
C_4H_{10}	5.4×10^{7}[a]	136.0	4.661
C_2H_2	5.1×10^{7}[a]	192.4	4.105
CH_3CN	4.4×10^{6}[a]	229.3	6.887
CO_2	1.3×10^{6}[a]	216.6	9.020
C_6H_6	1.0×10^{6}[b]	279.1	9.300

[a] Lavvas et al. (2008a,b).
[b] Vuitton et al. (2008).

characterized by its pure-component parameters: the number of segments m, the segment diameter σ (Å) and the segment energy of interaction ϵ/k_B (K). The PC-SAFT is extended to mixtures using the Berthelot–Lorentz combining rule for the dispersive energy, resulting in a single binary parameter k_{ij}. The values of all these parameters are determined by comparison with experimental results. Our implementation of PC-SAFT consists of a set of FORTRAN 2008 object-oriented subroutines written from scratch. Our model has been validated in two ways. We compared its outputs with experimental unitary and binary mixtures data for vapor–liquid equilibrium (hereafter VLE), largely similar to those already used by Tan et al. (2013) with the exception of CH_4–C_2H_6 mixtures (see Luspay-Kuti et al., 2015). We also checked that SLE results were in good agreement with laboratory measurements (similar to the work of Maity (2003)). For instance we verified that we correctly reproduced the data of dissolution of dotriacontane in heptane at varying temperatures (see Fig. 1). Our pure-component parameters are mainly taken from Tan et al. (2013), who used their own optimized adjustments. The NIST database or other sources, like the PC-SAFT original paper by Gross and Sadowski (2001), complete the sample. Concerning CH_3CN, we used the parameters published by Spuhl et al. (2004) and decided to neglect the association terms in the Helmholtz energy since they only provide improvements of the order of a few percent (see for instance Table 7 of Spuhl et al., 2004). This correction remains small compared to the other uncertainties related to the present modeling approach (exact composition of the solvent, influence of the interaction parameter and validity[3] of Eq. (1)). Additionally, solubilities are very sensitive to the value of the interaction parameters k_{ij} which are not known for nitriles relevant to this study (Stevenson et al., 2015b). We did not find m, σ and ϵ/k_B for HCN in the literature. Thus, we determined our own values by fitting the VLE data published by Giauque and Ruehrwein (1939) (see their Table II). Our adjustment is compared to data from Giauque and Ruehrwein (1939) in Fig. 2. All the m, σ, and ϵ/k_B values used in this study are summarized in Table 2. PC-SAFT also needs interaction parameters k_{ij} to account for interspecies molecular interaction, which may not be included in the adopted expression of the Helmholtz energy. In general, these k_{ij} are derived from VLE experimental data and are related to binary mixtures. Table 3 summarizes the interaction parameters adopted here. It should be noted that C_2H_2, CO_2, and C_6H_6 parameters have been derived from laboratory measurements published by Neumann and Mann (1969), Cheung and Zander (1968) and Diez-y-Riega et al. (2014), respectively. The rather good agreement between our own model and experimental data is shown in Fig. 3. Concerning the dissolution of C_6H_6 in ethane, we recognize that the measured value by Malaska and Hodyss (2014) at 94 K disagrees somewhat with those determined by Diez-y-Riega et al. (2014) (see Fig. 3(c)) but we used the measurements derived from Diez-y-Riega et al. (2014) since they

[3] see Appendix A.

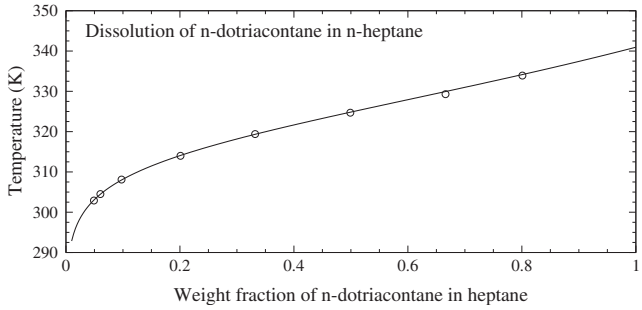

Fig. 1. Open circles: experimental solubility data for n-dotriacontane in n-heptane from Chang et al. (1983). Solid line: our model.

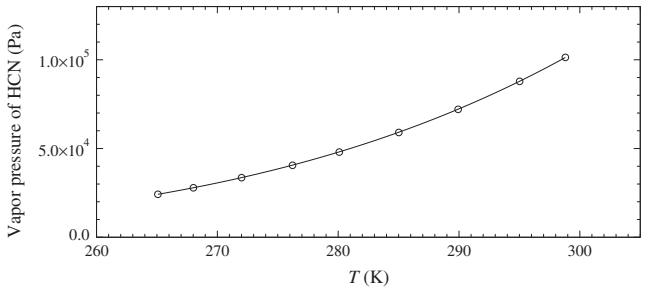

Fig. 2. Open circles: vapor pressure for a VLE of HCN, these experimental data are from Table II of Giauque and Ruehrwein (1939). Solid line: our best fit leading to the PC-SAFT parameters: $m = 2.434$, $\sigma = 3.2929$ Å and $\epsilon/k_B = 248.48$ K.

Table 2
The PC-SAFT pure-component parameters used in this study.

Name	m	σ (Å)	ϵ/k_B (K)	References
CH_4	1.000	3.7039	150.030	NIST, used by Tan et al. (2013)
N_2	1.2414	3.2992	89.2230	NIST, used by Tan et al. (2013)
C_2H_6	1.6114	3.5245	190.9926	NIST, used by Tan et al. (2013)
HCN	2.434	3.2929	248.48	This work
C_4H_{10}	2.6300	3.5100	190.900	Tamouza (2004)
C_2H_2	2.1569	2.9064	168.5506	Din (1962) used by Tan et al. (2013)
CH_3CN	2.2661	3.3587	313.04	Spuhl et al. (2004)
CO_2	2.0729	2.7852	169.210	Gross and Sadowski (2001)
C_6H_6	2.4653	3.6478	287.350	Gross and Sadowski (2001)

Table 3
The PC-SAFT binary interaction parameters k_{ij}. Only interactions between solute molecules and solvent ones have been taken into consideration in our model. By default, in the cases where dissolution data are not present in the literature, k_{ij} have been fixed to zero. For C_6H_6–C_2H_6, the best fit has been derived for a temperature dependent parameter. Solute-to-solute molecule interactions are ignored; this assumption can be considered a relatively safe assumption since solute abundances remains relatively low.

Name	CH_4	N_2	C_2H_6
CH_4	0	0.03 (1)	0.00 (1)
N_2		0	0.06 (2)
C_2H_6			0
HCN	0 (X)	0 (X)	0 (X)
C_4H_{10}	0.022 (4)	0 (X)	0 (X)
C_2H_2	0.115 (3)	0 (X)	0.105 (1)
CH_3CN	0 (X)	0 (X)	0 (X)
CO_2	0.085 (5)	0 (X)	0.13 (5)
C_6H_6	0.037 (4)	0 (X)	$-0.1388 + 15.070 \times 10^{-4} T$ (6)

(1) Tan et al. (2013); (2) this work, by fitting data from Gabis (1991) provided by Glein and Shock (2013); (3) this work, by fitting data from Neumann and Mann (1969) and Gross and Sadowski (2001); (5) this work, by fitting Cheung and Zander (1968) and previously used by Preston and Prausnitz (1970); (6) this work, by fitting data from Diez-y-Riega et al. (2014); (X) set to zero, as dissolution data were not found in the literature.

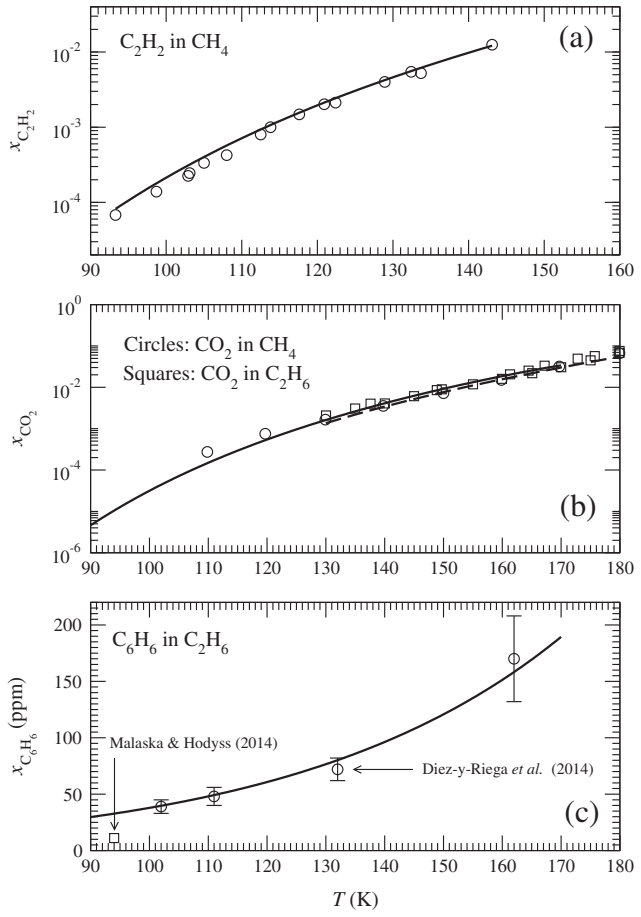

Fig. 3. Comparison between our solubility model and experimental data: the solubility of the considered species in a solvent (CH_4 or C_2H_6) is plotted as a function of temperature. (a) Mole fraction of dissolved acetylene in methane, the observed values have been taken in Neumann and Mann (1969) and the solid line represents our model. (b) The measured mole fraction of CO_2 dissolved in methane (circles) and in ethane (squares). (c) Dissolution of benzene (in ppm) in ethane, experimental data are from Diez-y-Riega et al. (2014) (circles) and Malaska and Hodyss (2014) (the square at 94 K).

were acquired over a temperature range and provide the necessary parameters for our PC-SAFT model. All unavailable interaction parameters have been set to zero.

2.2. The model for the evaporite layers thickness

The above-described model of liquid solutions provides only the number of moles of the various involved compounds that precipitate. Here we aim to estimate the thickness of the deposited layers; for this purpose, we thus need a model for the molar volumes of relevant species.

If during the time step Δt the precipitated quantities of organic matter are Δn_i (in mol), the resulting thickness Δe (in m) of the layer deposited over one square meter is given by $\Delta e = \sum_{i=1}^{N_{sat}} \Delta n_i \times V_{i,m}$. In this equation N_{sat} denotes the number of species that reach saturation during Δt, and $V_{i,m}$ represents the molar volume (in $m^3\ mol^{-1}$) of the solid i. It should be noted that inter-species possible interactions that could induce a deviation from the molar volume additivity and/or the problem of mechanical compaction are neglected. Hence, organic matter is assumed to form monocrystal structures, leaving no empty spaces in the evaporite layer as could be found in a porous medium. In that sense, the thicknesses calculated here are minimum values.

The molar volumes employed here are derived from the lattice parameters of the crystal cells of the organic compounds. For species where different crystal structures were experimentally observed, we chose the one stable at the temperature conditions found at the surface of Titan (*i.e.* 90–95 K). Table 4 brings together the crystal structures used in our model, which were measured at Earth ground atmospheric pressure. In the case where the volumes of the crystal cells were published for different temperatures, we verified that the influence of temperature variations on derived molar volumes is small enough to be ignored in our range of interest. The possible influence of pressure should be weak as the pressure at Titan's surface is ~1.5 bar; we evaluated its influence by means of a quantum chemical calculations along with the density functional theory (DFT). We found in general that the density of organic crystals decreases less than 1% over pressure ranges from 1 bar to 100 bar. C_2H_2, C_6H_6 and C_4H_{10} are exceptions for which the respective decreases were of −1.21%, −4.76% and −8.46%. We therefore conclude, as expected, that pressure variations are minor factors in the context of our work. The adopted molar volumes are listed in Table 5, slight differences between these molar volumes and those published in Cornet et al. (2015) are explained by a tentative correction to account for the temperature influence on the molar volumes in their paper (given at 91.5 K instead of 90 K). In addition, the difference in the mass density of CO_2 between the two studies is due to an error in the molar mass used for conversion to density (reported as 40 g mol^{-1} instead of 44 g mol^{-1}).

3. Evaporite structure: a 1D model

3.1. Evaporite formation scenario

The formation of any evaporite layer requires a sequence of wet and dry periods. During the wet episode, methane and/or ethane rains dissolve the solid organics encountered along their runoff at the ground, and then finally they fill the lacustrine depressions. The subsequent dry period produces the evaporation of the solvents, and thus the formation of evaporites. The resulting vertical distribution of species depends on both the initial composition of the mixture and the individual concentrations at saturation. In this context, the precipitation of solid organics from the atmosphere in the form of exotic snows or hails has been supposed to have either taken place prior to the flowing episode or have happened at the same time as the runoff. However, any solid organic atmospheric precipitation that occurs during the evaporation process would complicate the global picture of the evaporitic layer formation as it would increase the abundances of certain dissolved species. The production of organics at the surface, or even in the satellite interior, cannot be excluded, although clear evidence for such processes are not available. These still speculative phenomena could provide an organic stratum prior to any rainfall.

The sequence of dry-wet periods can span over just a single year if driven by Titan's seasonal effect. Alternatively, the formation of observed putative evaporites observed by Barnes et al. (2011) and MacKenzie et al. (2014) could be the consequence of the climate change over much longer timescales. However, the map of evaporite distribution published by MacKenzie et al. (2014) (see their Fig. 2). is globally consistent with the latitudinal distribution of methane rains obtained by Rannou et al. (2006) (see our Fig. 4). The largest number of deposits is concentrated in polar regions where the highest cumulative rainfall is predicted to occur, whereas the 5-μm-bright material detected by MacKenzie et al. (2014) in the equatorial region (*i.e.* around $\lambda \sim -30°$) is consistent with the low, but non-zero, methane precipitation rates found by

Table 4
Cell parameters of the crystal of the different molecular solids, observed to be stable at the temperature range of Titan's surface, 90–95 K. The temperature listed in the fifth column is used to experimentally determine the cell parameters.

Name	a (Å)	b (Å)	c (Å)	β (°)	Ref
HCN	4.13	4.85	4.34	90	Dietrich et al. (1975) and Dulmage and Lipscomb (1951)
C_4H_{10}	4.1463	7.629	8.169	118.656	Refson and Pawley (1986)
C_2H_2	6.198	6.023	5.578	90	McMullan et al. (1992)
CH_3CN	6.05	5.24	7.79	90	Antson et al. (1987)
CO_2	5.624	5.624	5.624	90	Etters and Kuchta (1989) and Simon (1980)
C_6H_6	7.384	9.416	6.757	90	Craven et al. (1993)

Table 5
The densities and derived molar volumes of the crystal structures of the different molecular solids, observed stable in the temperature range 90–95 K.

Name	ρ_{solid} (g cm^{-3})	Molar mass (g mol^{-1})	$V_{i,m}$ (m^3 mol^{-1})
HCN	1.03	27.0253	2.624×10^{-5}
C_4H_{10}	0.851	58.1222	6.830×10^{-5}
C_2H_2	0.831	26.0373	3.133×10^{-5}
CH_3CN	1.10	41.0519	3.732×10^{-5}
CO_2	1.643	44.0095	2.679×10^{-5}
C_6H_6	1.104	78.1118	7.075×10^{-5}

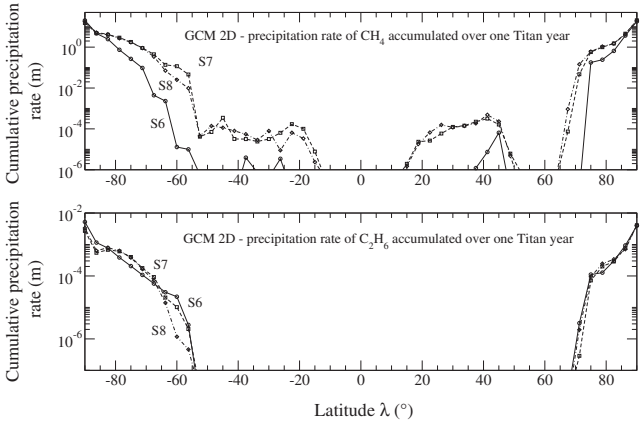

Fig. 4. (a) The cumulative precipitations (in meters) of methane as a function of Titan's latitude, computed by Rannou et al. (2006). (b) The same quantity for ethane. In both cases, labels S6, S7, and S8 correspond to various assumptions concerning the GCM 2D model inputs (*e.g.* thermal inertia and lake fraction at poles).

Rannou et al. (2006) and observational evidence Turtle et al. (2011) and Barnes et al. (2013).

Following Rannou et al.'s numerical simulations, the precipitation rate of CH_4 poleward from $\pm 80°$, ranges between 1 and 20 m per Titan year. In the case of ethane, this rate is much lower with values ranging from 3×10^{-4} to 5×10^{-3} m per Titan year. These numbers yield formation times for a column of liquid methane with a height of 100 m to be between 5 and 100 Titan years. Much longer periods of time are needed for ethane: the accumulation of a column of 100 m of ethane would take 20,000–300,000 Titan years.

However, these timescales of lake replenishment have to be considered as an upper limit because for one particular lake, as on Earth, the liquid catchment area (*i.e.* the drainage basin) is much more extended than the lakebed (*i.e.* the lacustrine depression) itself. For instance, an examination of Fig. 1 of Barnes et al. (2011) allows the reader to see that a collecting area with a surface ten (or even more) times that of the bed is quite common. The larger the surface of the drainage basin is, the shorter the lakebed replenishment time is. With a relatively large drainage basin, a replenishment timescale shorter than one Titan year is plausible.

In this work, we adopt a "standard" initial liquid depth of 100 m which is broadly consistent with the bathymetry of Ligeia Mare derived from altimetry measurements by Mastrogiuseppe et al. (2014). Besides, the computed evaporite layer structures could be easily rescaled to other initial liquid depths by applying a simple rule of proportionality. For example, a lake initially filled only with 10 m would correspond to a final layer tenfold thinner.

In the last decade, the application of GCMs has contributed much to our understanding of Titan's climate history and evolution. However, it is not straightforward, if even possible, to quantitatively compare all published GCM results because assumptions associated with each model differ significantly from one study to another. For instance, the microphysics required to approach realistic precipitation rates have been implemented in only two investigations (Tokano et al., 2001; Rannou et al., 2006); the radiative transfer could be based either on a two-stream model (e.g. GCM by Rannou et al., 2006; Tokano, 2009b) or on a gray atmosphere (e.g. GCM by Mitchell et al., 2011; Schneider et al., 2012); the dimensionality is either 2 or 3; and the methane reservoir could be considered finite or infinite. Most studies focus mainly on the predicted cloud activity, which presents the advantage of applicability to observational constraints. Unfortunately, the reported simulations cannot be taken at face value to derive cumulative methane/ethane precipitation rates. If we look at one of the most recent works, *i.e.* Schneider et al. (2012), and more specifically to their Fig. 1b in which the net evaporation rate $(E - P)$ has been plotted, a succession of wet and dry periods can be clearly seen at Titan's poles. Nevertheless, polar dry periods appear to undergo evaporation rates $(E - P) \sim 0$ mm day^{-1}, whereas slightly positive $(E - P)$'s seem to occur at latitudes around $\pm 30°$. At the first glance, this seems to be in contradiction with the evaporite distribution found by MacKenzie et al. (2014). However, Schneider et al. (2012) hypothesized a total methane content equivalent to 12 m of global liquid methane, and their results are averaged over 25 Titan years, which could erase the temporal fluctuations.

If we accept all the reservations mentioned above, and if we take cumulative methane precipitation rates computed by Rannou et al. (2006), then the existence (at least ephemerally) of local topological depressions filled by several tens of meters deep liquid methane looks plausible. Though the model is substantially different (microphysics is not included and the methane reservoir is finite), results from Schneider et al. (2012) lead to a similar conclusion. Mitri et al. (2007) have proposed estimations of hydrocarbon evaporation rates based on an equation originally published by Fairall et al. (1996). For instance, they found for a pure methane liquid layer an evaporation rate of $\sim 5 \times 10^3$ kg m^{-2} yr^{-1}; a value that yields to ~ 10 terrestrial years for the complete evaporation of a column of 100 m of liquid methane. This estimation is clearly compatible with the duration of a Titan season (*i.e.* ~ 7 Earth years) and allows the evaporation of a transient methane lake within that time period. The same authors obtained an evaporation rate of 1.5×10^3 kg m^{-2} yr^{-1} for a mixture of 35% of CH_4, 60% of ethane and 5% of nitrogen, an acceptable range. We note that Tokano (2009a) used the same prescription for his limnological study. Under slightly different conditions (no wind), Luspay-Kuti et al. (2012, 2015) obtained similar evaporation rates between $\sim 0.5 \times 10^{-4}$ and $\sim 2 \times 10^{-4}$ kg m^{-2} s^{-1} (equivalent to 1.58–6.31×10^3 kg m^{-2} yr^{-1}) in experimental simulations, depending on the actual content of ethane. In any case, the evaporation of several tens of meters deep hydrocarbon lake is likely possible within a few Titan months. Hence, the formation of at least a thin layer of evaporite is compatible with what we know about evaporation

Table 6
The solubility (in mole fraction) of considered solutes at $T = 90$ K and under 1.5 bar for an ideal solution and with our PC-SAFT based model. The solvent is only composed of either methane or ethane, e_{100} represents the final thickness of evaporites after the evaporation of an initial column of 100 m of liquid. These thicknesses were computed with PC-SAFT model solubilities. The notation $x \times 10^y = x(y)$ is used for conveniency.

Name	Ideal solution	PC-SAFT pure CH_4	PC-SAFT pure C_2H_6	e_{100} (m) pure CH_4	e_{100} (m) pure C_2H_6
HCN	6.46 (−4)	3.52 (−7)	4.64 (−5)	2.59 (−5)	2.65 (−3)
C_4H_{10}	1.26 (−1)	1.67 (−3)	9.14 (−2)	3.20 (−1)	13.6
C_2H_2	5.40 (−2)	4.84 (−5)	5.21 (−4)	4.26 (−3)	3.56 (−2)
CH_3CN	3.73 (−3)	4.27 (−8)	1.87 (−5)	4.47 (−6)	1.55 (−3)
CO_2	8.72 (−4)	2.45 (−6)	4.37 (−6)	1.84 (−4)	2.55 (−4)
C_6H_6	2.20 (−4)	7.20 (−9)	2.97 (−5)	1.43 (−6)	4.58 (−3)
Total thickness	(m)			0.324	13.65

rates, and it is plausible that the formation of the evaporites observed by Cassini have occured during the Titan's past. Some authors consider alternative mechanisms for the formation of features that are classified as "evaporites", which we discuss in more detail in Section 5.

Our model, based on PC-SAFT, has been mainly validated using data from solid organic dissolution where the solvent (methane or ethane) comprised the major components. However, our model has not been formally validated for very high concentration of solutes, *i.e.* for circumstances where the sum of their mole fractions is larger than ∼50%. We have then chosen to stop the evaporation algorithm when $\sum_{k(\text{solutes})} x_k > 0.5$. In practice, this criterion has been satisfied at the very end of the evaporation, *i.e.* when the ratio of the remaining volume and of the initial volume was approximately between 10^{-4} and 10^{-8}, depending on the particular composition adopted at the starting time. In fact, along the evaporation process the mole fraction of the solvent is nearly constant. Roughly, when a number of moles Δn are removed from the solvent by evaporation, a similar amount Δn of organics saturate and settled to the lakebed.

At the very end of the evaporation (*i.e.* during the last timestep), the remaining liquid is assumed to evaporate, and the total amount of still-dissolved compounds are deposited on the lakebed. In our model, when this evaporite final layer is composed of several species, they are assumed to be perfectly mixed.

3.2. The maximum thickness of evaporite: a first approach

Solution theory enables our model to estimate the allowed maximum thickness. For a given volume of liquid, the concentration at saturation of the considered compound gives the maximum quantity of matter that can be dissolved. Then, if we assume that all evaporite components are initially present in the solution at their saturation abundances, then the algorithm implemented in our model provides the thickness of the corresponding deposition. Table 6 shows the resulting depths, denoted e_{100}, corresponding to an initial height of solvent of 100 m. Unsurprisingly, ethane leads to greater final thicknesses because this molecule is a much better solvent than methane for the expected hydrocarbon solutes available to a Titan lake system. The resulting total thickness are respectively 0.324 and 13.65 m, for CH_4 and C_2H_6. The question remains, however, how easy it is to meet the conditions for the simultaneous saturations of all species. In other words, is the atmospheric photochemistry able to provide large enough quantities of organics to allow saturation in the lakes?

In Table 8, we estimated the dimensions of the catchment basins required to dissolve enough solid organics for the lake to reach saturation, for each investigated solute produced at the rates computed by Lavvas et al. (2008a,b) and accumulated during one Titan year. In this scenario, solid organics fall from the atmosphere (in the form of snows or hail) and would be washed into the lake with rainfall runoff flowing to the local topographic minimum, the lake. For idealized disk-shaped basins, we list the dimensions as a function of lake radius in Table 8 for either CH_4 or C_2H_6 playing the role of solvent. Different liquid depths H of the central are also considered. The lake itself is supposed to cover an area of 1 m^2. The computed radii correspond then to the catchment basin size required to get the saturation in a volume of $H \times 1$ (m^3) of liquid hydrocarbons.

HCN and C_4H_{10}, the solutes with respectively the smallest and largest mole fractions at saturation, need the smallest and the largest collecting area according to PC-SAFT calculation (see Table 6). More interestingly, these calculations indicate that butane is so soluble that reaching saturation requires an unreasonably large basin. In the most favorable case where methane is the solvent, for a diameter of ∼20 km (typical of some northern lakes (see Fig. 1 of Barnes et al., 2011)), and the initial depth fixed to 1 m, the drainage basin for butane must have a radius larger than the radius of Titan itself. In contrast, the saturation concentration of HCN is reached in a similar lake when this compound is drained over an area with a radius around 26 km while the assumed lake has a radius of 10 km.

Given the numbers reported in Table 8, we can safely conclude that all of the solutes considered in this study cannot be simultaneously at saturation in the initial state (*i.e.* before a significant evaporation episode) for a given lake. In addition, if the fraction of surface covered by evaporite in polar regions can be as high as ∼10% (see for instance Fig. 3 of MacKenzie et al., 2014), the average catchment area can only have a radius of 1.78 m for a central lake of 1 m^2 (a disk with a radius of 1.78 m has an area of ∼10 m^2). This value is lower than the majority of radii given in Table 8, indicating the improbability of lakes being saturated in their initial state. Thus we can firmly state that the thicknesses mentioned above, 0.324 and 13.65 m, are largely an overestimate if we impose a timescale of one Titan year. However, in Section 3.3, we will discuss a mechanism for repeated dissolution–evaporation–deposition that could overcome these limitations.

3.3. The possible 1D structure of evaporites

The structures of evaporitic deposit left at a lakebed after the entire evaporation of an assumed 100 m-high column of liquid have been computed. The results shown in Fig. 5 can be rescaled for any other initial liquid height. Two solvents have been employed: pure methane and pure ethane. In panel (a) of Fig. 5 the initial mixtures of dissolved organics are set by fixing the concentration of the most abundant species (*i.e.* HCN) to its value at saturation (*i.e.* 3.52×10^{-9}, see Table 6) while the abundances of other compounds are derived by scaling to the atmospheric production rates; the result is the "type A" mixture in Table 7. As a consequence, the initial total mole fraction of solutes reaches only

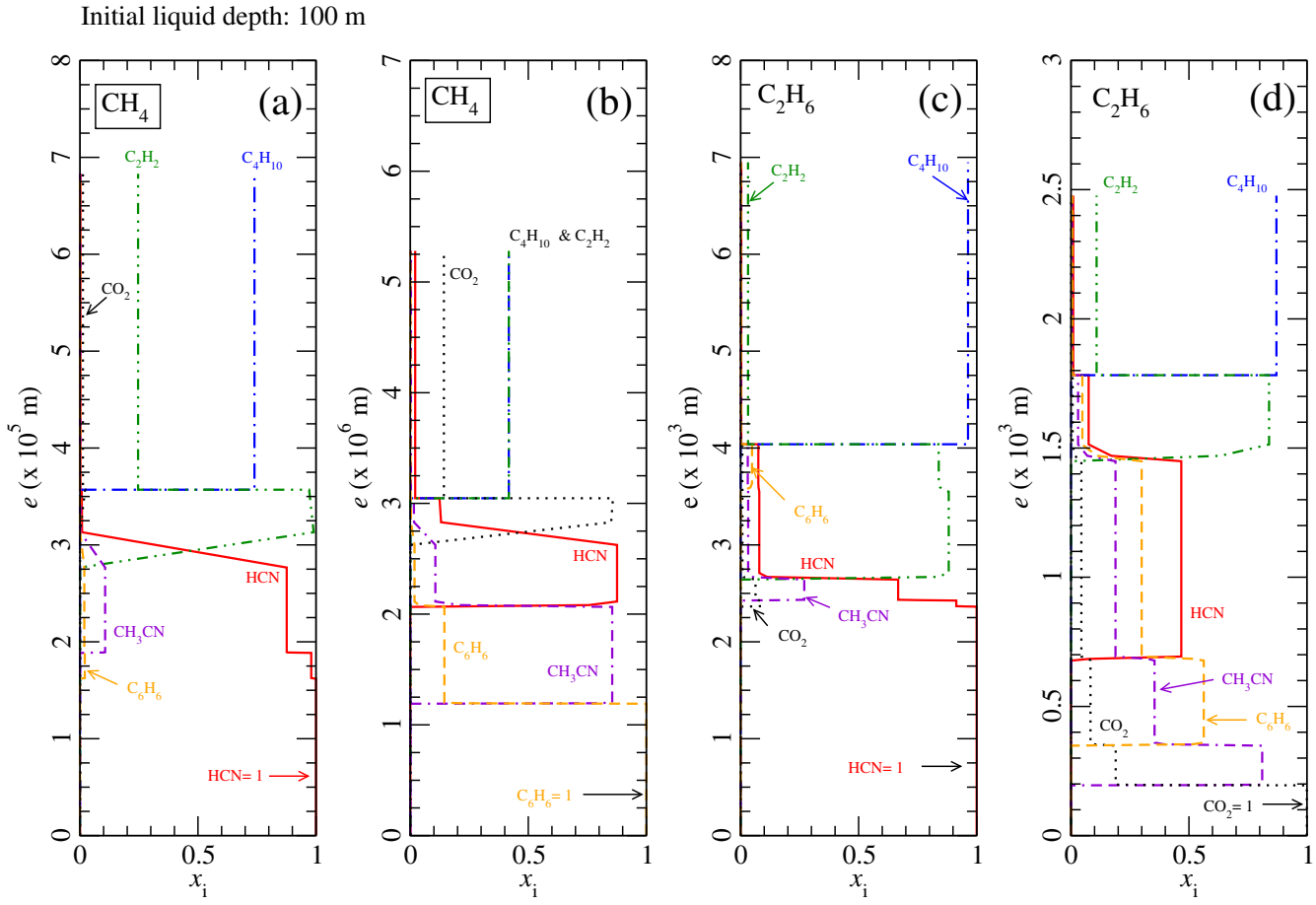

Fig. 5. 1D structure of evaporite layers, computed from an initial liquid depth of 100 m. The *y*-axis represents the height *e* of the resulting deposit over the non-soluble substrate. The *x*-axis shows the mole fractions x_i of the differing species at a given height. Two solvents are considered: methane (panels (a) and (b)), and ethane (panels (c) and (d)). In simulations reported in panels (a) and (c), the assumed initial mixture of solutes has a mole fraction of HCN (the most abundant species in atmospheric precipitation) set to its value at saturation in the considered solvent, and other concentration are derived by a scaling to atmospheric production rates. The results plotted in panels (b) and (d), have been obtained by adopting uniform solute concentrations, fixed to the lowest mole fraction at saturation.

Table 7
The initial mixtures of solutes taken into account. The entire set of compositions is divided into four types. Types A and B are used with a methane rich solvent whereas types C and D correspond to when ethane is the dominant solvent component. All abundances are expressed in mole fraction of the initial solution.

Species	Type A	Type B	Type C	Type D
HCN	3.519×10^{-7}	7.199×10^{-9}	4.635×10^{-5}	4.370×10^{-6}
C_4H_{10}	1.462×10^{-7}	7.199×10^{-9}	1.925×10^{-5}	4.370×10^{-6}
C_2H_2	1.381×10^{-7}	7.199×10^{-9}	1.818×10^{-5}	4.370×10^{-6}
CH_3CN	1.191×10^{-8}	7.199×10^{-9}	1.569×10^{-6}	4.370×10^{-6}
CO_2	3.519×10^{-9}	7.199×10^{-9}	4.635×10^{-7}	4.370×10^{-6}
C_6H_6	2.707×10^{-9}	7.199×10^{-9}	3.565×10^{-7}	4.370×10^{-6}

Table 8
Radius (in m) of possible idealized "catchment basins" of solid organics required to ensure the saturation of a given species in a column of solvent (CH_4 or C_2H_6) which height is *H*, and with a cross-section of 1 m^2 (corresponding to a disk with a radius of 0.56 m). All the computations were performed assuming an atmospheric precipitation timespan of one Titan year.

Name	CH_4 $H = 100$ m	CH_4 $H = 10$ m	CH_4 $H = 1$ m	C_2H_6 $H = 10$ m
HCN	15.18	4.799	1.518	48.41
C_4H_{10}	1621	512.5	162.06	3334
C_2H_2	284.2	89.88	28.42	259.0
CH_3CN	28.72	9.081	2.872	167.1
CO_2	400.2	126.5	40.02	148.7
C_6H_6	24.75	7.826	2.475	441.9

6.54×10^{-7}, a value that can be converted to a deposit thickness of a few tens of micrometers (6.83×10^{-5} m).

As already emphasized in PAP1, the most soluble species, *i.e.* C_4H_{10} and C_2H_2, remain dissolved until the very end of the evaporation process. Thus, these species dominate the final, top layer of the deposit. We noticed that the last droplet of solution to be evaporated contains the entire amount of dissolved C_4H_{10} and C_2H_2, around 50% of the volume of dissolved material. This is due to the small total amount of solute and the high solubilities of C_4H_{10} and C_2H_2 and explains the final vertical parts of the curves in the top of Fig. 5(a). Alternatively, the least soluble compounds (dominantly, for this mixture, HCN) are buried below the C_4H_{10}- and C_2H_2-enriched top layer.

The treatment of the "last droplet to be evaporated" is worth special attention. Indeed, our model has not been validated in situations where the solvent becomes a minor species of the "solution". Thus, we have simply adopted a principle of a well-mixed last layer, which is reflected in the top vertical parts of curves in Fig. 5(a) (and other panels). We therefore ignore possible segregation effects (presently unknown) that could occur during the late stages of evaporation. However, we are aware that different species can precipitate under different crystallographic phases leading

to an inhomogeneous mixture. This aspect will be the subject of a point of discussion further on in the paper.

Although the "type A" mixture is more realistic, we also use an uniform initial distribution of solutes ("type B" mixture displayed in Table 7). With this mixture, we eliminate the effect of the initial mixing ratios on the evaporite structure. HCN is no longer the solely dominant buried species; CH_3CN and C_6H_6 play a prominent role in this scenario. While butane and acetylene are still the major compounds of the external layer, carbon dioxide appears to reach abundances around 14%.

We also examine pure ethane as the solvent in the "type C" and "type D" mixtures of Table 7. Mixture "C" has an initial mixture corresponding to the most abundant species in precipitation (*i.e.* HCN) taken at its saturation. The initial solution for mixture "D" is similar to "type B" in that the uniform initial mole fractions are used: 4.37×10^{-6}, the lowest concentration at saturation of our set of solutes, *i.e.* that of CO_2. The results for these mixtures are displayed in Fig. 5(c) and (d), respectively, where the scale factor attached to the *y*-axis is 10^{-3}, meaning a depth of the order of a few millimeters. Solutions with methane (types "A" and "B") produce only micron-deep layers.

In the case where initial abundances are scaled to respective precipitation rates ("type C", Fig. 5(c)), the structure can be generally described as a layer of less solubles compounds (*i.e.* the nitriles CH_3CN and HCN) topped by a layer of butane. Comparison to Fig. 5 (a) shows unambiguously that the ethane-based mixture favors butane while the methane-based mixture favors acetylene in the surface layer. When uniform initial fractions are assumed (see mixture "type D" in Table 7), butane remains the most abundant species at the surface but leaves some space for C_2H_2. Not surprisingly, the interior structure is more complex with a non-negligible role of carbon dioxide and benzene.

If we focus on the external layer, these computations employing our new model based on PC-SAFT confirm the tendencies found in PAP1. However, we find here that the total thickness of the deposits is on the order of a few microns for a methane-rich solvent and a several millimeters for an ethane-rich solvent. In addition, when initial abundances of solutes are scaled to precipitation rates for either solvent, HCN seems to be the dominant buried species.

In order to assess the possible influence of dissolved N_2, we introduce an amount of nitrogen fixed at 10% of the current quantity of either CH_4 or C_2H_6. This mixing ratio seems realistic according to the current literature (Cordier et al., 2009, 2013a; Glein and Shock, 2013; Tan et al., 2013; Luspay-Kuti et al., 2015). Our results do not significantly differ with the inclusion of N_2 in the four mixture types. For instance, the resulting sequence of a 1D model of evaporites deposit structure remains essentially unchanged when the fraction of N_2 in the solvent (mainly composed by CH_4) is increased from 0.00 to 0.20. The most important change is a decrease of ~15% of the abundance of C_2H_2 in the top layer while an increase of the C_4H_{10} mole fraction of ~7% is found. This general low sensitivity to dissolved nitrogen abundances is not a surprise because the PC-SAFT interaction parameters k_{ij} between N_2 and the introduced solvent were set to zero due to the lack of relevant data. We emphasize, nevertheless, that except in the case of very strong interaction between these species, the role of N_2 should be of small importance, due to its relatively small abundance in the solutions.

Up to this point, all the simulated deposits were implicitly formed over an insoluble substrate. This approach is particularly relevant if this substrate is made of water ice and/or long chain hydrocarbons. Nevertheless, one can well imagine lakebeds successively flooding and drying year after year. If the atmospheric products are still the same in nature and quantities from one year to the next, we can expect an accumulation of evaporite at the bottom of these lakebeds. Additionally, liquid flowing into the system can re-dissolve, at least partially, the strata formed in previous cycles. We represent the end-member scenario where liquid runoff does not dissolve previously-formed evaporite layers in panels (a), (b) and (c) in Fig. 6, which could happen if the liquid runoff is too fast over the deposits. However, for liquid entering the system that is in contact with the deposits long enough to dissolve the evaporite (experiments by Malaska and Hodyss, 2014, give credence to this assumption), panels (d), (e) and (f) depict the evolution of evaporite layers. Around ~50% of the top layer formed during the previous year is brought into solution. As shown above, the most soluble species build the external layer of evaporite (deposited during some previous epochs). They are then the first "re-dissolved" material such that the current liquid solution becomes more enriched in the most soluble compounds. This leads to a secondary surface layer over-enriched in butane and/or acetylene (see panel (e) in Fig. 6). This process can be repeated from year to year, yielding to a very thick layer of the most soluble species (Fig. 6(f)), though the process might be limited by the saturation points of the solutes and the quantity of solvent running off.

Alternatively, if a much larger quantity of material is dissolved, for instance if all the deposited organics during the past year are redissolved, then, the new layers deposited in the next evaporation event are much thicker. In all cases, the dissolution of the previously formed layer increases the thickness of the external layers. This effect, however, is limited by the concentration at saturation and the average annual precipitation of liquid methane/ethane.

Regardless of the initial composition scenario, the surface layer of evaporite could be composed by a mixture of butane and acetylene. In addition, this top layer appears to be relatively thick compared to the depth of the whole deposit. With multi-annual repetition of the dissolution–evaporation process, the top butane–acetylene rich layer tends to grow in thickness. In Fig. 5, the uniform mole fractions of C_2H_2 and C_4H_{10} are only relevant on average. Indeed, it is extremely likely that these two species precipitate separately, each one in its own crystallographic phase. An homogeneous phase of C_2H_2–C_4H_{10} would imply the existence of something resembling an acetylene–butane "co-crystal" yet unknown but similar to what has been observed by Vu et al. (2014) for ethane and benzene. In addition, even if this kind of system exists, a perfectly homogeneous layer would require relative abundances of C_2H_2 and C_4H_{10} in agreement with the allowed stoichiometry of the "co-crystal". Thus, if butane and acetylene are present, the existence of a biphasic system seems more likely, and the structure of the top layer of evaporite could be similar to that depicted in Fig. 7, although the scales of heterogeneities are unknown.

The pebbles observed at *Huygens* landing site were probably formed by mechanical erosion and required relatively powerful liquid currents to flow in Titan's rivers (Tomasko et al., 2005). In contrast, evaporation in small lakes and ponds is a more gentle process but would also leave some irregularities like pebbles, evaporitic polygonal crusts, macroscopic crystals, that could produce high radar brightness as it has been also speculated in the case of channels observed by the Cassini RADAR (Le Gall et al., 2010). Indeed, on Earth, Devil's Golf Course (Death Valley, California) or Lucero Lake (White Sands National Monument, New Mexico) offer examples of evaporitic formations that show a several tenths of centimeters in size rugosity. Although these structures were largely due to erosion, there is no reason to ensure that this situation does not occur on Titan. Hence, the RADAR brightness of evaporites (see Barnes et al., 2011, Section 3) could be explained by processes occurring during either the lacustrine basin formation or the formation of evaporite deposits.

Unfortunately, we did not find frequency-dependent permittivity for solid butane and acetylene in the literature. However, since

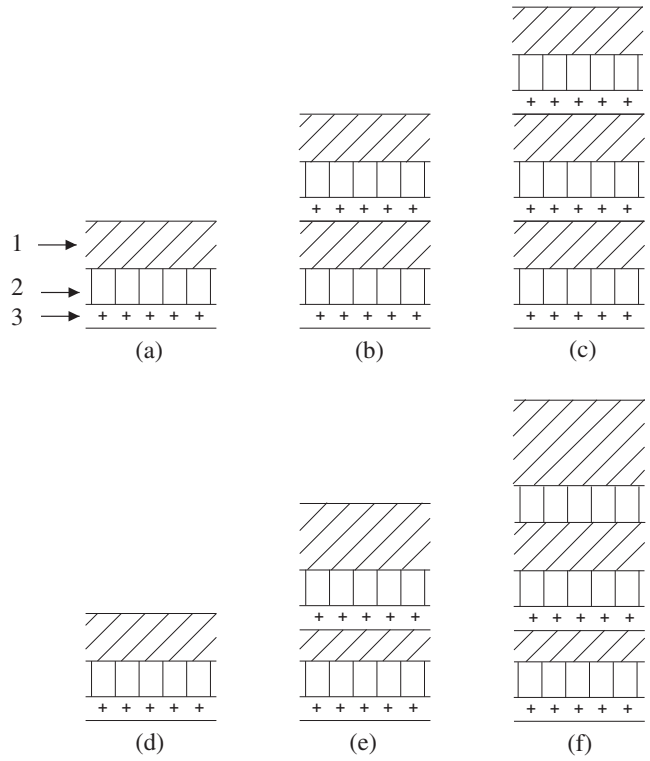

Fig. 6. Sketches of two scenarios of evaporites formation: three species (labeled 1, 2 and 3) are assumed for the sake of clarity. Both rows illustrate the evolution of a lakebed's evaporite layers over a period of three drying and evaporating cycles. The series (a), (b), and (c) corresponds to the accumulation of layers without any dissolution of the substrates deposited during the past years. At the bottom, the series (d), (e) and (f) presents schematically the evolution of evaporite layers if redissolution of previously laid-down layers is allowed to occur (in this example, between (e) and (f) only the two previous external layers were redissolved).

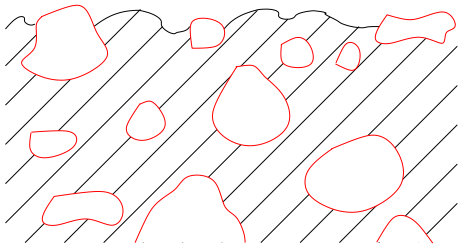

Fig. 7. Scheme of the plausible top layer structure of Titan's evaporite. The hatched area corresponds to a matrix made of the most abundant compound (forming a first macroscopic crystallographic phase), blank zones are composed by the less abundant, this corresponds to a second macroscopic phase. These heterogeneities have an effect on RADAR backscatter only if their scale is at least comparable to RADAR wavelength.

C_2H_2 and C_4H_{10} are both non-polar molecules, their polarizability provides the main contribution to the permittivity of their solid forms. We obtained the static permittivity $\epsilon_{r,0}$ at 195 K for both species ($\epsilon_{r,0}(C_4H_{10}) = 1.942$ and $\epsilon_{r,0}(C_2H_2) = 2.4841$) from *Handbook* (Lide, 1974). The difference in these values suggests substantially different permittivities in the microwave domain of the Cassini RADAR. We have shown that the thickness of evaporite can be as large as several tens of centimeters or even several meters, much larger than the wavelength of the Cassini RADAR (*i.e.* 2.18 cm) and therefore potentially affecting the RADAR signal. The observed RADAR brightness can be also caused by a layering but probably more likely by heterogeneities as depicted in Fig. 7.

In summary, the RADAR brightness at the evaporite (Barnes et al., 2011), if not produced by centimeter-sized surface roughness, could be also caused by heterogeneities within the top layer produced by the existence of at least two crystallographic phases. The subsurface horizons generated by stratification of evaporite (see Fig. 5) could also contribute to the effect, but the formation of plane interfaces between layers could be more difficult.

4. Evaporite deposits structure: a 2D model

Barnes et al. (2009, 2011) and MacKenzie et al. (2014) observed evaporite deposits along the periphery of lakebeds. The signal at 5 μm shows a gradient that could be explained by changes in chemical composition and/or thickness of the deposited organic material. On Earth, the combination of drought and increased water demand has produced significant drops in water levels of the well-known reservoirs Lake Mead and lake Powell. Consequently, "bathtub rings" have appeared along the shores of these lakes. These structures, mainly made of calcium carbonate, are observable in pictures taken from space (see for instance Barnes et al., 2009, Fig. 7). Similarly-formed "bathtub rings" around lakes on Titan are probably more complex due to the variety and different properties of the organic compounds involved. Consequently, these particular formations could be unique through the Solar System. Thus, a better understanding of evaporite formation is desirable.

For the sake of simplicity, we have adopted axisymmetric topography, as sketched out in Fig. 8. The bottom of the lakebed is represented by a disk-shaped flat terrain of radius R_1. This zone is surrounded by sloping ground that extends between the radii R_1 and $R_2 > R_1$. The value R_2 corresponds to the area covered by a volume with initial liquid depth H_0. Mastrogiuseppe et al. (2014) have performed bathymetric measurements along a RADAR track acquired during a nadir-looking altimetry flyby above Ligeia Mare. This sea is much larger than the class of lakes we are interested in. We note, however, that the shallow slope of the seabed revealed by the global bathymetric profile (see Fig. 4 of Mastrogiuseppe et al., 2014) generally agrees with the slope scheme we adopt here. Moreover, our results do not depend on the precise slope but rather on the exact shape of the shore terrain. In our baseline scenario, continuous evaporation removes liquid from the system while solid compounds are deposited in the bed. Parts of the lakebed deposits that are no longer immersed maintain their structure and composition until the end of the process. It is implicitly assumed that the kinetics of both precipitation and sedimentation are much faster than the kinetics of evaporation. Parts of the lakebed that are still submerged get covered by a growing layer of solid organics that stratifies gradually.

The properties and global characteristics of liquids mixing in Titan's lakes remain relatively unknown. Different physical processes can contribute to this mixing: vertical convection (Tokano, 2009a), tidal effects or global circulation (Tokano et al., 2014). In our approach, we chose to ignore the possible details of this mixing and instead consider two extreme cases: (1) only an efficient vertical mixing occurs and (2) a combined horizontal–vertical mixing scheme that ensures chemical homogeneity of the entire lake (see Fig. 8).

In case (1), the whole quantity of dissolved solutes contained in the initial column of liquid above a given point of the lake is precipitated on the bed following the behavior reported in our 1D model study (see Section 3). In such a case, the resulting composition of the evaporite deposition will show an uniform surface composition: only the depth will vary from one point to another. Locally the thickness of evaporite layers scales to the initial height of the local liquid column. No bathtub ring structures are expected

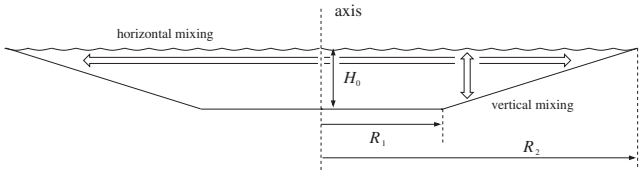

Fig. 8. Schematic cross-section of our idealized lakebed. We denote H_0 the initial liquid depth, R_1 and R_2 are defined in the text.

in case (1). Thus, observations of a Titan lakebed lacking evaporite rings could be understood as the mark of a weakly efficient horizontal mixing in the lake and/or evidence for an unsaturated solution.

In case (2), the time-dependent compositions and thickness of the deposits are easily computed by fixing the sizes of the lake to typical values, *i.e.* $R_1 = 15$ km, $R_2 = 30$ km (see for instance Fig. 1 panel C of Barnes et al., 2011) and an initial depth of $H_0 = 600$ m. This implies a shore slope of $\sim 2.3°$, similar to those reported in Table 9. The computation algorithm is divided in two main steps. First, for the corresponding total volume $V_{tot} = \pi H_0 (R_1^2 + R_2^2 + R_1 R_2)/3$, our thermodynamic model is employed to estimate the quantities of precipitated matter during each time step. The resulting outputs are then applied to the chosen particular geometry such that at each timestep, the total amount of over-saturated species is uniformly distributed over the immersed part of the bed. These operations are repeated until the solvent is exhausted.

The results are summarized in Fig. 9. The mixture types used for the 1D model are also used here. The solvents are pure methane (Fig. 9 panels (a) and (b)) and pure ethane (Fig. 9 panels (c) and (d)). For each solvent, two initial solutes compositions are considered: either the abundances are scaled to atmospheric precipitation rates (Fig. 9 panels (a) and (c)), or the initial mole fractions are all fixed to the smallest saturation value (Fig. 9 panels (b) and (d)). Unsurprisingly, the surface of the central part of the evaporite deposits, *i.e.* that which covers the flat bottom of the basin, has a composition dominated by butane and acetylene. This behavior is explained, as in the 1D results, by the large solubilities of these two species, which are thus able to remain dissolved until the very late stages of the liquid evaporation. During this last episode, the liquid stagnates above the bed bottom and the species, that are still dissolved, finally precipitate out. Clearly, this composition is consistent with the abundances of the top layers exhibited by the 1D model (see Fig. 5), although a slight difference is evident in the ethane solvent (Fig. 5(c)) where an almost pure butane region is surrounded by an acetylene rich crown.

The most external parts of the lacustrine basin are covered by a surface made of solid HCN when the solutes initial abundances are scaled to the atmospheric precipitation composition (see Fig. 9 panels (a) and (c)). In this scenario, the most plausible for an average lake, hydrogen cyanide is the most abundant dissolved compound though it is very poorly soluble. When the initial composition of solutes is uniform (Fig. 9 panels (b) and (d)), an external ring is made of either benzene (when CH_4 is the solvent, Fig. 9(b)) or carbon dioxide (when C_2H_6 is the solvent, Fig. 9(d)). These results indicate that the occurrence of an external HCN-rich ring would likely be caused by large initial content of the solution rather than a pure solubility effect. We emphasize that although HCN is clearly detected in the atmosphere (see for instance Vinatier et al., 2010; de Kok et al., 2014), its solubility in cryogenic solvents remains not well known, and values provided in this work are less reliable than those concerning other species, especially when the model outputs are compared to experimental works (see Section 2.1). Laboratory experiments are needed in order to determine the interaction parameters k_{ij}s related to HCN.

Table 9
Lake shore slopes derived from data published by Hayes et al. (2008) (Fig. 3, panel c). In this paper, the positions of the lakes are indicated by their respective abscissa along the RADAR track, *i.e.* "shore 1" is the one first crossed by the track. The central part of the "lake 1" bed has not been taken into consideration because of the lack of data. "Lake 1" and "lake 2" correspond respectively to features around ~140 and ~320 km along RADAR track in Fig. 3 of Hayes et al. (2008).

Object	Shore 1 Slope (in degrees)	Central region of the bed (in degrees)	Shore 2 Slope (in degrees)
Lake 1	1.812	–	1.773
Lake 2	4.445	0.420	3.180

Finally, between the outer portion (*i.e.* $r \gtrsim 22$ km) and the central area (*i.e.* $r \lesssim 15$ km) there lies a transitional zone that exhibits a chemically complex surface. Whatever the initial assumed composition, the resulting surface composition of evaporites appears to be "trimodal": a C_4H_{10}–C_2H_2 central region is bordered by a chemically complex narrow ring which is itself surrounded by an extended region where HCN is the dominant species (if the adopted atmospheric precipitations are representative of the actual weather conditions in Titan's troposphere). These conditions could either bring solutes to the lake directly from atmospheric fallout or wash the surrounding terrains and dissolve pre-existent solids that could cover these areas.

We underline that this chemically "trimodal" surface composition does not depend on the actual slope of the lacustrine basin shore. Indeed, a shore with a more gentle slope will be covered by thinner depositions, but will show more extended "bathtub rings", the aspect ratio being preserved. Narrower rings will be caused by steeper shores, again maintaining the aspect ratio. In terms of deposit thickness, low slopes correspond to shallow evaporite layers, whereas steep shores will exhibit thick strata.

The spectroscopic observation of all species involved in this study, is beyond the capabilities of an instrument like VIMS. However, the predicted "trimodal" surface composition of evaporite layers could be tentatively detected by VIMS if the spatial resolution is high enough (for instance $\lesssim 5$ km/pixel). The data spanning Ontario Lacus' evaporite-covered shorelines, analyzed by Barnes et al. (2009), have a high spatial resolution, as good as 330 m/pixel. These coastal features seem to be "bimodal" with two distinct zones (see Barnes et al., 2009, Fig. 4). After excluding several hypotheses (freezing, continental shelf, etc.), Barnes et al. (2009) proposed that the inner ring could be an intertidal zone showing exposed lake-bottom sediments. The external ring appears to have a low water–ice content, leading Barnes et al. (2009) to propose that it consists of fine-grained condensate, resulting of the evaporation of the liquid. These observations are consistent with our "trimodal" evaporation deposition. Indeed, in the case of Ontario Lacus, the liquid could still contain a large amount of solutes since it seems to be rich in ethane (Brown et al., 2008; Luspay-Kuti et al., 2015), a much more efficient solvent than methane. In our simulations, the central part of the deposit (see Fig. 9) is built up during the last stages of the evaporation, when butane and/or acetylene crystallize. Hence, the distinct two zones observed by Barnes et al. (2009) could correspond to two chemically different evaporite deposits: "unit 3" (the most external in Barnes et al. denomination) is perhaps composed of HCN while "unit 2" could be a "chemically complex" deposit. This interpretation is not mutually exclusive with that of an intertidal zone.

Also using VIMS data, Moriconi et al. (2010) have tentatively detected organic species within the rings observed around Ontario Lacus. They used the Spectral Angle Mapper technique to compare pixel spectra to the reference spectra of compounds of interest (C_2H_6, CH_4, C_4H_{10}, HCN, C_3H_8, C_2H_2 and C_6H_6). However, the definitive identification of surface compounds on Titan remains a matter of debate given the few opportunities left to see the surface with a

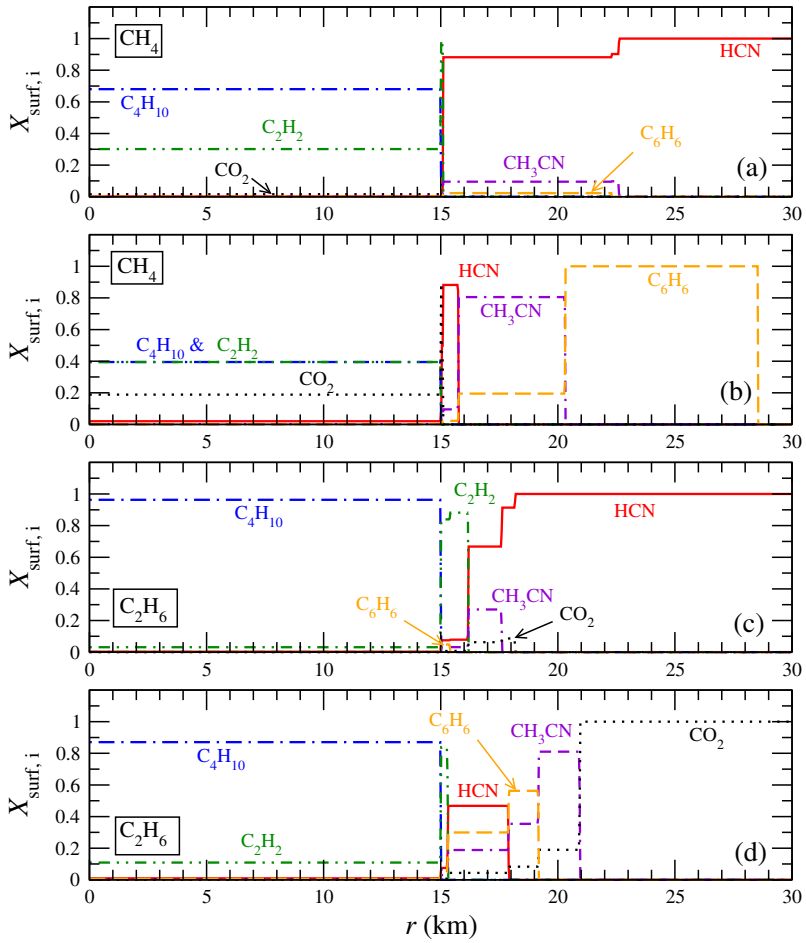

Fig. 9. Surface composition (in mole fraction) of a model lakebed with topography depicted in Fig. 8. The initial mixtures are those adopted for simulations reported in Fig. 5, *i.e.* in panels (a) and (b) the solvent is pure CH_4 while in panels (c) and (d) it is ethane. Two solute compositions are considered: the initial abundances are scaled to atmospheric precipitation rates (with HCN initially at saturation), corresponding to panels (a) and (c), and uniform abundances, as in panels (b) and (d). In order to be consistent with Fig. 5, species are represented by the same line style. The radius r represents the distance to the axis of the modeled lake basin.

reduced atmospheric contribution and an increased Signal-to-Noise Ratio with VIMS.

Nonetheless, the infrared data analyzed by Moriconi et al. (2010) appear to be compatible with the presence of C_4H_{10}, C_2H_2 and HCN within the area called "the ridge" by the authors (equivalent to unit 3 of the study of Barnes et al., 2009). The possible detection of species in liquid state under Titan's ground conditions, *i.e.* C_2H_6, CH_4 and C_3H_8, can be explained by either sediments still soaked in the corresponding liquid or an altimetric profile not as simple as that depicted in Fig. 8. Indeed, citing Lorenz et al. (2009); Moriconi et al. (2010) noted that the "ridge" could have a non-uniform elevation (see also Fig. 6 in Cornet et al., 2012). A lake shore altimetric profile with a changing slope could lead to a solid crystallization sequence within sporadic pools that could exist in the zone.

Globally, the findings of Moriconi et al. (2010) are in agreements with our predictions where C_4H_{10}, C_2H_2 and HCN appears to be the most abundant species at evaporites surface. Fig. 9 shows that C_6H_6 has a very discrete presence in scenarios where the initial compositions are scaled to atmospheric abundances (panels (a) and (c) in Fig. 9). Therefore, the non-detection of benzene can be interpreted as evidence that the composition of the atmospheric precipitation is similar to that computed by Lavvas et al. (2008a,b), as proposed in the interpretation of Moriconi et al. (2010). However, in their surface mapping of a 5.05-μm spectral feature on Titan's surface, Clark et al. (2010) shown that benzene could be present in a circular geological pattern (see Fig. 17.B of their study), which they interpreted as a dry lakebed. Unfortunately, this feature has not been imaged by the RADAR in order to confirm its exact geological nature, and mainly whether it pertains to the class of possible lakebeds or not.

Our model also predicts evaporite layer thickness. In Fig. 10, we have plotted the total thickness of the evaporite deposition in the scenario where solute abundances are scaled to production rate of solids (see Fig. 9) and using an ethane solvent. The central plateau is explained by the final deposition of C_4H_{10}, in agreement with the results of our 1D models (Fig. 5(c)). The change in slope observed between $r = 15$ km and 16 km is a consequence of the sudden saturation of acetylene (see Fig. 9(c)).

Fig. 10 is typical of the thickness distribution of evaporite deposits after one sequence of dissolution–evaporation. In Titan weather conditions, successive evaporation and flooding episodes can occur and thus drive thicker deposits via redissolution/precipitation mechanisms similar to those already discussed in Section 3.2.

5. Discussion

Throughout this article we have assumed that the main process that removes a solvent is evaporation. Several authors have discussed the possibility of fluids percolation within some porous

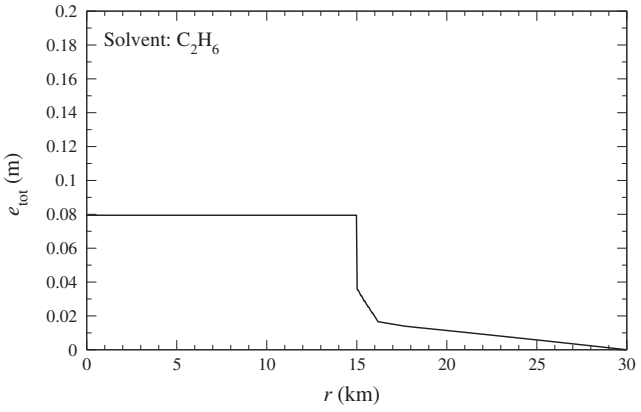

Fig. 10. The total thickness e_{tot} (in meter) of the resulting evaporite layer that appears after evaporation of the solvent. The adopted lakebed topography is described in Fig. 8, r (km) represents the typical radius of a lake initially containing solutes with abundances scaled to atmospheric precipitation rates (this model corresponds to what it is depicted by Fig. 9(c)).

regolith or terrain (Hayes et al., 2008; Choukroun and Sotin, 2012; MacKenzie et al., 2014). This process could be efficient only in the case where solid particles would not fill the regolith pores. A situation where the compounds belonging to the solvent could percolate, leaving behind initially dissolved species, seems particularly unrealistic since the pores would have very specific (and still unknown) properties; in addition, deposited layers at the lake bed would have to remain permeable to solutes, irrespective of its thickness. Nevertheless, we could wonder whether even in case of liquid percolation, the formation of evaporitic deposition could take place. Hence, if the bulk of the liquid, initially lying in a lacustrine depression, flows into a porous geologic formation instead of evaporate; at the end it will still remain a thin layer of liquid. The depth of this former layer depends on the wetting properties of the system solid substrate–liquid, namely the surface tensions liquid–vapor and liquid–solid (Butt et al., 2003), which are essentially unknown, although they do exist. A crude estimation of the possibly resulting depth of the coat of evaporite can be made. For that purpose, we assume a wetting film of a thickness around 1 mm. Table 6 provides the thickness equivalent to an initial depth of 100 m of saturated liquid. From these numbers, one can easily derive the possible thickness of the evaporite layer left after the evaporation of a final wetting film. One finds a thickness around a few microns, mainly due to butane. Thus, even if the geological substrate is porous, the formation of a fine evaporite layer remains possible.

All of our solubilities have been computed assuming a solvent that contains three major species: CH_4, C_2H_6 and N_2. This was clearly a reasonable assumption; however, it does not account for the potential role of a less abundant player like propane. Although photochemical models predict a relative precipitation rate of C_3H_8 one order of magnitude smaller than that of ethane (Lavvas et al., 2008b), propane could play a role in regions where it would be overabundant compared to its global average concentration. Brown et al. (2008), in their analysis of the 5-μm window, were not able to exclude the existence for a small amount of propane, butane and high-order alkanes in Ontario Lacus. Thus, we have calculated the mole fraction at saturation of considered solutes in pure C_3H_8. Unfortunately, among the PC-SAFT interaction parameters k_{ij} relevant for propane, the only one available is that of the couple (C_3H_8,C_2H_2) (taken from Tan et al., 2013), for others we used 0.0 (like in most cases involving C_2H_6 as a solvent). In general, for a solute X, adopting $k_{ij} = 0.0$ for both (C_2H_6, X) and (C_3H_8, X), we got a maximum solubility in propane roughly a factor of 2 higher than in ethane. This tendency is also found in the case of C_2H_2 where k_{ij} is known. The only noticeable exception is for CO_2; for this compound we use the $k_{ij} \neq 0.0$ determined for (C_2H_6, CO_2) (see Section 2), but we have not been able to draw any satisfactory conclusions. In short, the possible presence of some amount of propane could somewhat enhance the solubility of solid organics without changing essentially the formation scheme of evaporites.

It is difficult to compare our solubility estimations with previous works since the theoretical background (equilibrium with the atmosphere or not, the use of RST or PC-SAFT, etc.), the thermodynamical conditions (pressure and temperature) and the exact composition of the solvent and the solutes taken into account vary from one publication to another. For instance Dubouloz et al. (1989) and Cordier et al. (2013a) consider simultaneous equilibria of the liquid with solid organics, and the vapor phase of the atmosphere. Raulin (1987) consider a temperature of 94 K while we take 90 K, which is probably more realistic. In addition Raulin (1987) used a version of Eq. (1) that is slightly differ from our version, but the term introduced in their equation is questionable (see our discussion in Appendix A). A summary of solubilities found in previous works can be found in Cornet et al. (2015) (see their Table B.5). Making a detailed list of the explicit differences in the theoretical assumptions of each published model would not reveal any physical insight great enough to justify such an undertaking. However, one can notice that they have a significant dependence on free parameters in common. The values of these parameters are directly determined by adjustment on experimental data, as these are the best numbers currently available. There is never, however, a guarantee of their validity in the context of Titan. Sometimes the values are crudely estimated, like the δ_{ij} in the case of the RST, or a default value is adopted as is the case in Stevenson et al. (2015b) and in this work for nitrogen compounds (the k_{ij}'s are taken equal to zero for the nitrogen species). In this work, we made a substantial effort to get an agreement with available experimental data by adjusting free parameters. This could explain the differences between some previous works (Raulin, 1987; Dubouloz et al., 1989; Cordier et al., 2013a) and our results for C_2H_2, CO_2, and C_6H_6. We determined that a disagreement of the order of about a factor of ten remains acceptable. Recently Stevenson et al. (2015b) concentrated their experimental efforts on nitrogen compounds. As a general trend, they found HCN and CH_3CN less soluble than what we found. Nonetheless, the solubility of CH_3CN in pure methane at 94 K (see their Table 4) is close to our determination: both are around 10^{-8}. Other models provide higher values, *e.g.* COSMO-RS estimates around 10^{-7}. In the case of HCN, the output of the Stevenson et al.'s COSMO-RS model is not too far from our value with solubilities of the order of 10^{-7}–10^{-8}. The implementation of PC-SAFT by Stevenson et al. (2015b) yields values significantly smaller, with solubilities in the range of 10^{-11}–10^{-12}. We recall that this could be explained by parameters that are dissimilar between the two models: m, σ and ϵ were directly determined with laboratory data in our work (see our Fig. 2) while Stevenson et al. (2015b) used other sources. More importantly, together with Stevenson et al. (2015b), we did not find data which allow the determination of the k_{ij}'s for HCN and CH_3CN. As emphasized by Stevenson et al. (2015b) (see their Tables 11 and 12) results depend drastically on k_{ij}'s; this problem could only be solved by future theoretical chemistry simulations or experimental measurements. Finally, the "global picture" of the evaporite structure does not seem to depend on the chosen model: very soluble species (like C_2H_2 and C_4H_{10}, which are among the most soluble with an RST or PC-SAFT approach) should be predominant at the surface of the central region of the deposit, whereas less solubles like HCN (all models seem to indicate that nitrogen bearing molecules are

poorly soluble) should lay along the former shoreline. For instance, estimates of HCN solubility much smaller than ours must reenforce the tendency we found.

"Tholins", generated in laboratory experiments, have long been proposed as Titan's aerosol analogs (Khare et al., 1984; Sagan et al., 1992). Numerous experimental works show that they are complex combinations of C–N–H molecules, with a molecular weight ranging between ∼100 to ∼800 daltons (Imanaka et al., 2004; McDonald et al., 1994; Sarker et al., 2003; Nna-Mvondo et al., 2013). In addition, they have been found to be very poorly soluble in nonpolar solvents (McKay, 1996; Coll et al., 2001). Tholins are macromolecules much larger than those considered in this study. In the frame of the PC-SAFT theory, the segment number m increases with the molecular size, whereas the hard-core segment diameter σ and the segment–segment interaction energy parameter ϵ/k_B remain approximately constant. This behavior can be easily understood: m represents the number of "hard spheres" that are assumed to compose the molecule in question. One can check this tendency in Table 6 of Tihic et al. (2008), where the ratio m/MW (MW stands for the molecular weight) stays around ∼0.02 for a collection of polymers. At the same time, σ and ϵ/k_B keep values around ∼4 Å and ∼250 K respectively.

For a sensitivity analysis, we tried increasing progressively the segment number of butane, from its standard value 2.63 to 7 ($m = 8$ has lead to a non-convergence of PC-SAFT, due to an unphysical situation), leaving σ and ϵ/k_B unchanged. The solubility of butane has been computed in ethane at 90 K, under 1.5 bar. We found that the concentration of butane would fall from 9.14×10^{-2} (in mole fraction) to 1.04×10^{-3} (in our hypothetical $m = 7$ case). In other words the solubility is very sensitive to the value of m and decreases by several order of magnitude when m is increased by only a few units. More sophisticated numerical experiments (*e.g.* in which m is estimated using a group-contribution approach for a complex macromolecule, see Tihic et al., 2008) yield a similar conclusion.

As already emphasized in PAP1, the enthalpy of melting that appears in Eq. (1) has a strong influence of the resulting solubility. This enthalpy can be estimated using a group-contribution method (see for instance Joback, 1984); the relevant equation proposed in Appendix C of Poling et al. (2007) has the following form

$$\Delta H_m = -0.88 + \sum_k N_k(hmk) \times 0.004184 \qquad (2)$$

where N_k is the number of groups (–CH_3, –OH, ...) of type k, and the hmk's represent the corresponding contributions to the enthalpy; they are provided by dedicated tables. For the majority of these groups — first of all CH_3, CH_2 and CH — the hmk's are positive. Thus the general tendency is an increase of ΔH_m with the size of molecules leading to lower solubility. In PAP1, the authors discussed the case of the most simple molecule of the hydrazine family; (identified by Quirico et al., 2008, to be one of the possible components of tholins) CH_3CH_3N–CH_2; and also cyanoacetylene HC_3N. Unfortunately, for both molecules, we were not be able to find in the literature values of even estimations for their PC-SAFT parameters. Then, we cannot, for this moment, improve the solubility estimations computed in PAP1 for this particular species.

However, Titan's atmospheric aerosols that fall on its surface (Barth and Toon, 2006; Larson et al., 2014) –and that could be similar to tholins– have probably a very low solubility. Therefore, a layer of these aerosols may compose the lakebed, and most likely below the layers of butane and acetylene and those of HCN and CH_3CN. The "tholins" might be buried at the bottom of the evaporitic deposition or compose the external part of the bathtub.

Present knowledge of the Titan's surface chemical composition suffers from a lack of data. Brown et al. (2008) published clues in favor of the presence of the ethane in Ontario Lacus. In their work, Clark et al. (2010) identified benzene but they could not disentangle spectral signature of HC_3N and CO_2 while C_2H_2 has not been detected and CH_3CN could explain some spectral features. Beyond this, we have to keep in mind that *in situ* exploration could bring some surprises: for instance, in their experimental work, Vu et al. (2014) and Cable et al. (2014) have explored the formation of benzene–ethane co-crystals. Moreover, even if the low temperature of the surface disfavors the kinetics of chemical reactions, cosmics-ray particles could penetrate down to the surface (Sagan and Thompson, 1984; Zhou et al., 2010) and their energy deposition (see Molina-Cuberos et al., 1999) could speed-up some simple organics processes that could lead to the emergence of unexpected species over geological timescales. In short, molecules taken into account in this work as evaporites are supported by photochemical models, but we cannot exclude that future investigations or possible *in situ* exploration will reveal chemical surprises.

As emphasized in PAP1, possible turbidity is a major issue in our context. The presence of impurities may play a role in the nucleation of precipitating organics providing favorable nucleation sites, and they may also contribute to the deposits left on the ground after evaporation of the liquid. The authors of PAP1 have recalled that the laws of thermodynamics favor the heterogeneous nucleation since the cost in energy is lower in the case of a heterogeneous process compared to a homogeneous one, but Malaska and Hodyss (2013) observed, in their experiments, volume precipitation of benzene (M. Malaska, private communication) suggesting homogeneous precipitation. This unexpected phenomenon could be explained either by the presence of impurities in the liquid or by a very smooth internal surface of the experimental cell. Among our few observational constraints, Brown et al. (2008), using observation through the 5-μm window, have noticed that Ontario Lacus appears to be filled with a liquid free of particles larger than a few micrometers. In addition, in their study of Ligeia Mare Mastrogiuseppe et al. (2014) have also pointed out that the low attenuation of the RADAR signal is compatible with a ternary mixture of nitrogen, methane and ethane, excluding, after discussion, the possibility of significant turbidity caused by suspended scatterers. Despite this, the question of turbidity remains an open issue that could be answered by future space missions.

In their study of the geographical distribution of evaporite candidates, MacKenzie et al. (2014) noticed a clear lack of 5-μm-bright material in the south pole district. This observation cannot be explained by water snow falling from the atmosphere since Titan's atmosphere is particularly poor in water (Coustenis et al., 1998; de Kok et al., 2007; Moreno et al., 2012; Cottini et al., 2012). Therefore, MacKenzie et al. (2014) have proposed three possible explanations to this observation: (1) the evaporites layers could have been buried; being covered by a cap of aerosols, (2) the liquid could have percolated to a subsurface reservoir through a porous regolith, or (3) that there just haven't ever been deep, long-lived liquids at the south pole. However, the explanation offered by aerosols settling appears much more unlikely than percolation, since that implies a probable disappearance of difference between south zones which seems to be water–ice rich, and those consistent with water–ice in VIMS data.

Two alternative origins of this lack of southward evaporites can be proposed. First, if organic solutes are mainly produced in the atmosphere, one can imagine the existence of a low production rate above the south polar regions, phenomenon caused by the photochemistry itself and/or by properties of the atmospheric circulation that could disfavor the south pole. This hypothesis is supported by the asymmetrical distribution of lakes, which could be explained by the insolation asymmetry caused by Saturn's system orbital properties (Aharonson et al., 2009; Lora and Mitchell, 2015). Second, due to the high concentrations at saturation of potential

solutes into ethane (see Table 6), this solvent, by running off over the surface, could dissolve and trap almost the entire amount of solid organics that have been fallen from the atmosphere over the south polar region. The fact that Ontario Lacus is recognized to be enriched in ethane (Brown et al., 2008; Luspay-Kuti et al., 2015) strengthens this interpretation. Moreover, the RADAR very low loss tangent observed in Ligeia Mare by Mastrogiuseppe et al. (2014), contrasts with the much stronger absorption estimated at Ontario Lacus (Hayes et al., 2010); this fact could be interpreted as the consequence of the solvation of more absorbing compounds like long chain hydrocarbons, aromatics and nitriles (Mastrogiuseppe et al., 2014). Order of magnitude evaluations can be also invoked. For that purpose, we employed the least-square fit, established by Lorenz et al. (2008), that provides the average depth of the Earth's 20 largest lakes, as a function of their size (*i.e.* the square root of their surface area). Applied to Ontario Lacus, this law suggests an average depth of ~200 m, for an adopted surface area of 15,600 km^2; finally leading to an approximate total volume of $\sim 4 \times 10^{12}$ m^3. If we assume a content made of pure ethane, this volume corresponds to $\sim 10^{17}$ mol, mole fractions at saturation gathered in Table 6 allow estimations of maximum quantities of solutes that can be contained in Ontario. On another side, we have estimated the total quantities of organic solids settled to the regions further south than Ontario Lacus, which represent a total area of about 2×10^{12} m^2; this, during a period equal to a Titan's year. To do so, we simply have multiplied the rates coming from Lavvas et al. (2008b), by both the considered area and the chosen period of time. The results show that the maximum dissolved quantities, allowed by our model, exceed by a factor of $\sim 10^3$–10^4 the amounts of potential solutes that are assumed to fall from the atmosphere according to photochemistry models. Thanks to Cassini RADAR data, Ventura et al. (2012) derived a more realistic average depth for Ontario Lacus, around ten times lower than our crude estimation. Obviously, even a much shallower lake does not alter our conclusion. Therefore, our scenario, postulating that the south polar regions are currently dominated by liquid ethane that could host the major part of soluble species, appears plausible.

6. Conclusion

We have developed a new model of dissolution based on the up-to-date theory called PC-SAFT. This model takes into account recent laboratory measurements. As a by-product, we have determined the PC-SAFT parameters for HCN. The absence of available interaction parameters k_{ij} for some species, among them HCN, encourages further experimental work on the solubility determinations in cryogenic solvents.

With our model, we have also computed the possible vertical structure of evaporite deposits. These 1-D simulations confirm the result already published in PAP1: butane and acetylene are good candidates for species that could compose the surface of evaporite. In addition, we found that a couple of compounds could form a thick external layer; and due to the combination of the existence of two crystallographic phases and of the rather thick layer, this external C_4H_{10}–C_2H_2 enriched layer could explain the RADAR brightness of evaporites, if the scale of the produced heterogeneities is similar or larger than the RADAR wavelength. We have also shown that the seasonal cycle may offer a mechanism which leads to a growth of evaporite thickness only limited by atmospheric production of organics. Thanks to our solubility calculation, we also suggest that ethane-enriched south pole lake Ontario Lacus could have trapped a large quantity of solutes, and this would explain – at least partially – the lack of evaporite in the south polar regions.

Under realistic conditions, with our 2-D model we confirm the possibility of the formation of "bathtub rings", showing a complex chemical composition. However our model suggests the possible existence of "trimodal bathtub ring compositions when the entire evaporation is completed. Our predictions are in agreement with past observations of Ontario Lacus by Barnes et al. (2009) and Moriconi et al. (2010) and suggest the need of a future Titan's space mission involving a lander, partly focused on the exploration of the lakes shores, where the chemical diversity is clearly high (Stevenson et al., 2015a).

Acknowledgments

We thank Giuseppe Mitri for scientific discussion. TC is funded by the ESA Research Fellowship in Space Science Programme. The authors acknowledge financial support from the ESAC Faculty (ESAC-358 proposal). Finally, we thank the anonymous Reviewers who improved the clarity of the paper with their remarks and comments.

Appendix A. The validity of the equation of liquid–solid equilibrium

The solubility calculations, presented throughout this paper, rely in Eq. (1), which is – as already mentioned in PAP1 – an approximation. The rigorous expression is given by (see for instance, annex of Maity, 2003)

$$\ln(\Gamma_i X_i^{sat}) = \underbrace{-\frac{\Delta H_{i,m}}{RT_{i,m}}\left(\frac{T_{i,m}}{T}-1\right)}_{(1)} \underbrace{-\frac{1}{RT}\int_P^{P_i^{sat}}\left(V_{i,m}^S - V_{i,m}^L\right)dP}_{(2)} \underbrace{-\frac{1}{RT}\int_T^{T_{i,m}}\left(C_{p,i}^S - C_{p,i}^L\right)dT}_{(3)} + \underbrace{\frac{1}{T}\int_T^{T_{i,m}}\left(C_{p,i}^S - C_{p,i}^L\right)\frac{dT}{T}}_{(4)} \quad (A.1)$$

and one can legitimately wonder if terms (2), (3) and (4) have a global contribution negligible compared to term (1) or not. It is very striking to note that experimental data can be nicely reproduced even without these terms (see Figs. 1 and 3). It is probably safe then to assume that either terms 2, 3, and 4 have a tiny contribution or that their role is included in the effect of the interaction parameters k_{ij}. Nonetheless, we have tentatively tried to estimate the values of terms (2)–(4). We found in the literature laboratory measurements for the specific heats $C_{p,i}^S$ of some involved solids: C_4H_{10}, C_6H_6, CH_3-CN and HCN (respectively in Aston and Messerly, 1940; Oliver et al., 1948; Putnam et al., 1965; Giauque and Ruehrwein, 1939); and the specific heats $C_{p,i}^L$ of the subcooled liquids can – at least in principle – be evaluated by the use of PC-SAFT. This equation of state only provides their quantities if the Helmholtz energy (or equivalently the specific heat $C_{p,i}^{id}$ of the corresponding ideal gas) is known. Hence, we have estimated these $C_{p,i}^{id}$ using the group-contribution method developed by Joback (1984) and Joback and Reid (1987) and summarized by Poling et al. (2007). In order to test the validity of this approach, we compared the speed of sound

$$c_{sound} = \sqrt{\frac{C_p}{C_v}\frac{1}{k_T \rho}} \quad (A.2)$$

obtained by this method with experimental results for some cryogenic liquids. The agreement was not good enough to allow a firm validation of the method. The current development status of our model does not then permit reliable estimation for terms (3) and (4).

On one hand, measured molar volumes $V^S_{i,m}$ of solids are available (see Table 5); on the other hand the molar volume $V^L_{i,m}$ of subcooled liquids can be computed by PC-SAFT because it is not required to know the Helmholtz energy of the corresponding ideal gas. The vapor pressures P^{sat} are clearly negligible compared to the ambient pressure of ~1.5 bar, in addition solids and liquids have in general a very low compressibility, that way term (2) in Eq. (A.1) is not significantly different from $\sim|V^S_{i,m} - V^L_{i,m}| \times P/RT$. Then, for the solid species involved in this work, the term (1) ranges between ~1 and ~10, while $|V^S_{i,m} - V^L_{i,m}| \times P/RT$ has values of the order of $\sim 10^{-4}$–10^{-3}. We conclude that term (2) is negligible, whereas the precise role of the terms (3) and (4) remains questionable, even if the k_{ij}'s could partly mimic their effect.

References

Aharonson, O. et al., 2009. An asymmetric distribution of lakes on Titan as a possible consequence of orbital forcing. Nat. Geosci. 2, 851–854. http://dx.doi.org/10.1038/ngeo698.

Antson, O., Tilli, K., Andersen, N., 1987. Neutron powder diffraction study of deuterated β-acetonitrile. Acta Crystallogr., 296–301

Aston, J., Messerly, G.H., 1940. The heat capacity and entropy, heats of fusion and vaporization and the vapor pressure of n-butane. J. Am. Chem. Soc. 62, 1917–1923.

Barnes, J.W. et al., 2009. Shoreline features of Titan's Ontario Lacus from Cassini/VIMS observations. Icarus 201, 217–225. http://dx.doi.org/10.1016/j.icarus.2008.12.028.

Barnes, J.W. et al., 2011. Organic sedimentary deposits in Titan's dry lakebeds: Probable evaporite. Icarus 216, 136–140. http://dx.doi.org/10.1016/j.icarus.2011.08.022.

Barnes, J.W. et al., 2013. Precipitation-induced surface brightenings seen on Titan by Cassini VIMS and ISS. Planet. Sci. 2, 1–22.

Barth, E.L., Toon, O.B., 2006. Methane, ethane, and mixed clouds in Titan's atmosphere: Properties derived from microphysical modeling. Icarus 182, 230–250. http://dx.doi.org/10.1016/j.icarus.2005.12.017.

Brown, R.H. et al., 2008. The identification of liquid ethane in Titan's Ontario Lacus. Nature 454, 607–610. http://dx.doi.org/10.1038/nature07100.

Butt, H.J., Graf, K., Kappl, M., 2003. Physics and Chemistry of Interfaces. Wiley-VCH Verlag, Weinheim.

Cable, M.L. et al., 2014. Experimental determination of the kinetics of formation of the benzene–ethane co-crystal and implications for Titan. Geophys. Res. Lett. 41, 5396–5401. http://dx.doi.org/10.1002/2014GL060531.

Chang, S., Maurey, J.R., Pummer, W.J., 1983. J. Chem. Eng. Data 28, 187–189.

Cheung, H., Zander, E.H., 1968. Chem. Eng. Progr.; Symp. Ser. No 88 64, 34.

Choukroun, M., Sotin, C., 2012. Is Titan's shape caused by its meteorology and carbon cycle? Geophys. Res. Lett. 39, L04201. http://dx.doi.org/10.1029/2011GL050747.

Clark, R.N. et al., 2010. Detection and mapping of hydrocarbon deposits on Titan. J. Geophys. Res. (Planets) 115, E10005. http://dx.doi.org/10.1029/2009JE003369.

Coll, P. et al., 2001. Chemical and optical behaviour of tholins, laboratory analogues of Titan aerosols. Adv. Space Res. 27, 289–297. http://dx.doi.org/10.1016/S0273-1177(01)00060-6.

Cordier, D. et al., 2009. An estimate of the chemical composition of Titan's lakes. Astrophys. J. Lett. 707, L128–L131. http://dx.doi.org/10.1088/0004-637X/707/2/L128. Available from: <0911.1860>.

Cordier, D. et al., 2012. Titan's lakes chemical composition: Sources of uncertainties and variability. Planet. Space Sci. 61, 99–107. http://dx.doi.org/10.1016/j.pss.2011.05.009. Available from: <1104.2131>.

Cordier, D. et al., 2013a. Erratum: "An estimate of the chemical composition of Titan's lakes". Astrophys. J. Lett. 768, L23. http://dx.doi.org/10.1088/2041-8205/768/1/L23.

Cordier, D., Barnes, J.W., Ferreira, A.G., 2013b. On the chemical composition of Titan's dry lakebed evaporites. Icarus 226 (2), 1431–1437. http://dx.doi.org/10.1016/j.icarus.2013.07.026.

Cornet, T. et al., 2012. Geomorphological significance of Ontario Lacus on Titan: Integrated interpretation of Cassini VIMS, ISS and RADAR data and comparison with the Etosha Pan (Namibia). Icarus 218, 788–806. http://dx.doi.org/10.1016/j.icarus.2012.01.013.

Cornet, T. et al., 2015. Dissolution on Titan and on Earth: Toward the age of Titan's karstic landscapes. J. Geophys. Res. (Planets) 120, 1044–1074. http://dx.doi.org/10.1002/2014JE004738. Available from: <1505.08109>.

Cottini, V. et al., 2012. Water vapor in Titan's stratosphere from Cassini CIRS far-infrared spectra. Icarus 220, 855–862. http://dx.doi.org/10.1016/j.icarus.2012.06.014.

Coustenis, A. et al., 1998. Evidence for water vapor in Titan's atmosphere from ISO/SWS data. Astron. Astrophys. 336, L85–L89.

Craven, C. et al., 1993. The structure and dynamics of solid benzene. I. A neutron powder diffraction study of deuterated benzene from 4 K to the melting point. J. Chem. Phys. 98, 8236–8243.

de Kok, R. et al., 2007. Oxygen compounds in Titan's stratosphere as observed by Cassini CIRS. Icarus 186, 354–363. http://dx.doi.org/10.1016/j.icarus.2006.09.016.

de Kok, R.J. et al., 2014. HCN ice in Titan's high-altitude southern polar cloud. Nature 514, 65–67. http://dx.doi.org/10.1038/nature13789. Available from: <1410.5563>.

Dietrich, O., Mackenzie, G., Pawley, G., 1975. The structural phase transition in solid DCN. J. Phys. C: Solid State Phys. 8, L98–L102.

Diez-y-Riega, H. et al., 2014. Unsaturated hydrocarbons in the lakes of Titan: Benzene solubility in liquid ethane and methane at cryogenic temperatures. Planet Space Sci. 99, 28–35. http://dx.doi.org/10.1016/j.pss.2014.05.003.

Din, F., 1962. Thermodynamic Functions of Gases, vol. 2. Butterworth Inc., Washington.

Dubouloz, N. et al., 1989. Titan's hypothesized ocean properties – The influence of surface temperature and atmospheric composition uncertainties. Icarus 82, 81–96. http://dx.doi.org/10.1016/0019-1035(89)90025-0.

Dulmage, W., Lipscomb, W., 1951. The crystal structures of hydrogen cyanide, HCN. Acta Crystallogr. 4, 330–334.

Etters, R., Kuchta, B., 1989. Static and dynamic properties of solid CO_2 at various temperatures and pressures. J. Chem. Phys. 90, 4537–4541.

Fairall, C.W. et al., 1996. Bulk parameterization of air-sea fluxes for tropical ocean-global atmosphere coupled-ocean atmosphere response experiment. J. Geophys. Res. 101 (C2), 3747–3764.

Gabis, D.H., 1991. Liquid–Vapor Equilibrium at 90–160 K for Systems Containing Nitrogen, Methane, and Ethane. Ph.D. Thesis, Cornell Univ.

Giauque, W.F., Ruehrwein, R.A., 1939. The entropy of hydrogen cyanide. Heat capacity, heat of vaporization and vapor pressure. Hydrogen bond polymerization of the gas in chains of indefinite length. J. Am. Chem. Soc. 61, 2626–2633.

Glein, C.R., Shock, E.L., 2013. A geochemical model of non-ideal solutions in the methane–ethane–propane–nitrogen–acetylene system on Titan. Geochim. Cosmochim. Acta 115, 217–240. http://dx.doi.org/10.1016/j.gca.2013.03.030.

Gross, J., Sadowski, G., 2001. Perturbed-chain SAFT: An equation of state based on a perturbation theory for chain molecules. Ind. Eng. Chem. Res. 40, 1244–1260. http://dx.doi.org/10.1021/ie0003887.

Hayes, A. et al., 2008. Hydrocarbon lakes on Titan: Distribution and interaction with a porous regolith. Geophys. Res. Lett. 35, L09204. http://dx.doi.org/10.1029/2008GL033409.

Hayes, A.G. et al., 2010. Bathymetry and absorptivity of Titan's Ontario Lacus. J. Geophys. Res. (Planets) 115, 9009. http://dx.doi.org/10.1029/2009JE003557.

Imanaka, H. et al., 2004. Laboratory experiments of Titan tholin formed in cold plasma at various pressures: Implications for nitrogen-containing polycyclic aromatic compounds in Titan haze. Icarus 168, 344–366. http://dx.doi.org/10.1016/j.icarus.2003.12.014.

Joback, K.G., 1984. Unified Approach to Physical Property Estimation Using Multivariate Statistical Techniques. Ph.D. Thesis, Massachusetts Institute of Technology.

Joback, K.G., Reid, R.C., 1987. Chemical potential – A quantity in search of recognition. Chem. Eng. Commun. 57, 233–243.

Khare, B.N. et al., 1984. The organic aerosols of Titan. Adv. Space Res. 4, 59–68. http://dx.doi.org/10.1016/0273-1177(84)90545-3.

Larson, E.J.L., Toon, O.B., Friedson, A.J., 2014. Simulating Titan's aerosols in a three dimensional general circulation model. Icarus 243, 400–419. http://dx.doi.org/10.1016/j.icarus.2014.09.003.

Lavvas, P.P., Coustenis, A., Vardavas, I.M., 2008a. Coupling photochemistry with haze formation in Titan's atmosphere, Part I: Model description. Planet Space Sci. 56, 27–66. http://dx.doi.org/10.1016/j.pss.2007.05.026.

Lavvas, P.P., Coustenis, A., Vardavas, I.M., 2008b. Coupling photochemistry with haze formation in Titan's atmosphere, Part II: Results and validation with Cassini/Huygens data. Planet Space Sci. 56, 67–99. http://dx.doi.org/10.1016/j.pss.2007.05.027.

Le Gall, A. et al., 2010. Radar-bright channels on Titan. Icarus 207, 948–958. http://dx.doi.org/10.1016/j.icarus.2009.12.027.

Lide, D.P. (Ed.), 1974. CRC Handbook of Chemistry and Physics, 74th ed. CRC Press.

Lora, J.M., Mitchell, J.L., 2015. Titan's asymmetric lake distribution mediated by methane transport due to atmospheric eddies. Geophys. Res. Lett. 42, 6213–6220. http://dx.doi.org/10.1002/2015GL064912.

Lorenz, R.D. et al., 2008. Titan's inventory of organic surface materials. Geophys. Res. Lett. 35, L02406. http://dx.doi.org/10.1029/2007GL032118.

Lorenz, R.D. et al., 2009. Ontario Lacus: Brilliant observations of a Titan lake by the Cassini Cassini RADAR altimeter. In: Lunar and Planetary Science Conference, vol. 40, p. 1990.

Luspay-Kuti, A. et al., 2012. Experimental simulations of CH_4 evaporation on Titan. Geophys. Res. Lett. 39, 5, L23203.

Luspay-Kuti, A. et al., 2015. Experimental constraints on the composition and dynamics of Titan's polar lakes. Earth Planet. Sci. Lett. 410C, 75–83.

MacKenzie, S.M. et al., 2014. Evidence of Titan's climate history from evaporite distribution. Icarus 243, 191–207. http://dx.doi.org/10.1016/j.icarus.2014.08.022. Available from: <1408.2899>.

Maity, S.K., 2003. Modeling and Simulation of Solid–liquid Equilibrium by Perturbed-Chain Statistical Associating Fluid Theory. Master's Thesis, Indian Institute of Technology; Kharagpur, India.

Malaska, M. et al., 2012. Titan in a fume hood: Room-temperature simulation of a Titan evaporite playa using a multi-component mixture of organic compounds. In: Lunar and Planetary Science Conference. Lunar and Planetary Inst. Technical Report, vol. 43, p. 2139.

Malaska, M., Hodyss, R., 2013. Laboratory investigation of benzene dissolving in a Titan lake. LPI Contrib. 1719, 2744–2745.
Malaska, M.J., Hodyss, R., 2014. Dissolution of benzene, naphthalene, and biphenyl in a simulated Titan lake. Icarus 242, 74–81. http://dx.doi.org/10.1016/j.icarus.2014.07.022.
Mastrogiuseppe, M. et al., 2014. The bathymetry of a Titan sea. Geophys. Res. Lett. 41, 1432–1437. http://dx.doi.org/10.1002/2013GL058618.
McDonald, G.D. et al., 1994. Chemical investigation of Titan and Triton tholins. Icarus 108, 137–145. http://dx.doi.org/10.1006/icar.1994.1046.
McKay, C.P., 1996. Elemental composition, solubility, and optical properties of Titan's organic haze. Planet. Space Sci. 44, 741–747. http://dx.doi.org/10.1016/0032-0633(96)00009-8.
McMullan, R., Kvick, A., Popelier, P., 1992. Structures of cubic and orthorhombic phases of acetylene by single-crystal neutron diffraction. Acta Crystallogr. Sect. B Struct. Sci. 48, 726–731.
Mitchell, J.L. et al., 2011. Locally enhanced precipitation organized by planetary-scale waves on Titan. Nat. Geosci. 4, 589–592. http://dx.doi.org/10.1038/ngeo1219.
Mitri, G. et al., 2007. Hydrocarbon lakes on Titan. Icarus 186, 385–394. http://dx.doi.org/10.1016/j.icarus.2006.09.004.
Molina-Cuberos, G.J. et al., 1999. Ionization by cosmic rays of the atmosphere of Titan. Planet. Space Sci. 47, 1347–1354. http://dx.doi.org/10.1016/S0032-0633(99)00056-2.
Moreno, R. et al., 2012. The abundance, vertical distribution and origin of H_2O in Titan's atmosphere: Herschel observations and photochemical modelling. Icarus 221, 753–767. http://dx.doi.org/10.1016/j.icarus.2012.09.006.
Moriconi, M.L. et al., 2010. Characterization of Titan's Ontario Lacus region from Cassini/VIMS observations. Icarus 210, 823–831. http://dx.doi.org/10.1016/j.icarus.2010.07.023.
Neumann, A., Mann, R., 1969. Die Loslichkeit von festem Acetylen in flussigen Methan/Athylen-Mischungen. Chem. Ing. Tech. 41, 708–711.
Nna-Mvondo, D. et al., 2013. Thermal characterization of Titan's tholins by simultaneous TG-MS, DTA, DSC analysis. Planet. Space Sci. 85, 279–288. http://dx.doi.org/10.1016/j.pss.2013.06.025.
Oliver, G.D., Eaton, M., Huffman, H.M., 1948. The heat capacity, heat of fusion and entropy of benzene. J. Am. Chem. Soc. 70, 1502–1505.
Poling, B.E., Prausnitz, J.M., O'Connell, J., 2007. The Properties of Gases and Liquids, fifth ed. McGraw-Hill Professional, Englewood Cliffs.
Preston, G.T., Prausnitz, J.M., 1970. Thermodynamics of solid solubility in cryogenic solvents. Ind. Eng. Chem. Process Des. Develop 9, 264–271.
Putnam, W.E., McEachern, D.M., Kilpatrick, J.E., 1965. Entropy and related thermodynamic properties of acetonitrile. J. Chem. Phys. 42, 749–755.
Quirico, E. et al., 2008. New experimental constraints on the composition and structure of tholins. Icarus 198, 218–231. http://dx.doi.org/10.1016/j.icarus.2008.07.012.
Rannou, P. et al., 2006. The latitudinal distribution of clouds on Titan. Science 311, 201–205. http://dx.doi.org/10.1126/science.1118424.
Raulin, F., 1987. Organic chemistry in the oceans of Titan. Adv. Space Res. 7, 71–81. http://dx.doi.org/10.1016/0273-1177(87)90358-9.
Refson, K., Pawley, G., 1986. The structure and orientational disorder in solid n-butane by neutron powder diffraction. Acta Crystallogr., 402–410
Sagan, C., Thompson, W.R., 1984. Production and condensation of organic gases in the atmosphere of Titan. Icarus 59, 133–161. http://dx.doi.org/10.1016/0019-1035(84)90018-6.
Sagan, C., Thompson, W.R., Khare, B., 1992. Titan: A laboratory for prebiological organic chemistry. Acc. Chem. Res. 25, 286–292. http://dx.doi.org/10.1021/ar00019a003.
Sarker, N. et al., 2003. Titan aerosol analogues: Analysis of the nonvolatile tholins. Astrobiology 3, 719–726. http://dx.doi.org/10.1089/153110703322736042.
Schneider, T. et al., 2012. Polar methane accumulation and rainstorms on Titan from simulations of the methane cycle. Nature 481, 58–61. http://dx.doi.org/10.1038/nature10666.
Simon, A.P.K., 1980. Single-crystal refinement of the structure of carbon dioxide. Acta Crystallogr., 2750–2751
Spuhl, O. et al., 2004. Ind. Eng. Chem. Res. 43, 4457–4464.
Stevenson, J., Lunine, J., Clancy, P., 2015a. Membrane alternatives in worlds without oxygen: Creation of an azotosome. Sci. Adv. 1, e1400067. http://dx.doi.org/10.1126/sciadv.1400067.
Stevenson, J.M. et al., 2015b. Solvation of nitrogen compounds in Titan's seas, precipitates, and atmosphere. Icarus 256, 1–12. http://dx.doi.org/10.1016/j.icarus.2015.04.019.
Stofan, E.R. et al., 2007. The lakes of Titan. Nature 445, 61–64. http://dx.doi.org/10.1038/nature05438.
Stofan, E.R. et al., 2011. The Titan Mare Explorer Mission (TiME): A discovery mission to a Titan sea. In: EPSC-DPS Joint Meeting 2011, p. 909.
Tamouza, S.M., 2004. Utilisation prédictive de l'équation d'état SAFT. Ph.D. Thesis, Université de Paris XIII, France.
Tan, S.P. et al., 2015. Titans liquids: Exotic behavior and its implications on global fluid circulation. Icarus 250 (0), 64–75. http://dx.doi.org/10.1016/j.icarus.2014.11.029.
Tan, S.P., Kargel, J.S., Marion, G.M., 2013. Titan's atmosphere and surface liquid: New calculation using Statistical Associating Fluid Theory. Icarus 222, 53–72. http://dx.doi.org/10.1016/j.icarus.2012.10.032.
Tihic, A. et al., 2008. A predictive group-contribution simplified PC-SAFT equation of state: Application to polymer systems. Ind. Eng. Chem. Res. 47, 5092–5101.
Tokano, T. et al., 2001. Three-dimensional modeling of the tropospheric methane cycle on Titan. Icarus 153, 130–147. http://dx.doi.org/10.1006/icar.2001.6659.
Tokano, T., 2009a. Limnological structure of Titan's hydrocarbon lakes and its astrobiological implication. Astrobiology 9, 147–164. http://dx.doi.org/10.1089/ast.2007.0220.
Tokano, T., 2009b. Impact of seas/lakes on polar meteorology of Titan: Simulation by a coupled GCM-Sea model. Icarus 204, 619–636. http://dx.doi.org/10.1016/j.icarus.2009.07.032.
Tokano, T., Lorenz, R.D., Van Hoolst, T., 2014. Numerical simulation of tides and oceanic angular momentum of Titan's hydrocarbon seas. Icarus 242, 188–201. http://dx.doi.org/10.1016/j.icarus.2014.08.021.
Tomasko, M.G. et al., 2005. Rain, winds and haze during the Huygens probe's descent to Titan's surface. Nature 438, 765–778. http://dx.doi.org/10.1038/nature04126.
Turtle, E.P. et al., 2011. Rapid and extensive surface changes near Titan's equator: Evidence of april showers. Science 331, 1414–1417. http://dx.doi.org/10.1126/science.1201063.
Vinatier, S. et al., 2010. Analysis of Cassini/CIRS limb spectra of Titan acquired during the nominal mission. I. Hydrocarbons, nitriles and CO_2 vertical mixing ratio profiles. Icarus 205, 559–570. http://dx.doi.org/10.1016/j.icarus.2009.08.013.
Ventura, B. et al., 2012. Electromagnetic models and inversion techniques for Titan's Ontario Lacus depth estimation from Cassini RADAR data. Icarus 221, 960–969. http://dx.doi.org/10.1016/j.icarus.2012.09.011.
Vu, T.H. et al., 2014. Formation of a new benzene–ethane co-crystalline structure under cryogenic conditions. J. Phys. Chem. A 118, 4087–4094.
Vuitton, V., Yelle, R.V., Cui, J., 2008. Formation and distribution of benzene on Titan. J. Geophys. Res. (Planets) 113, 5007. http://dx.doi.org/10.1029/2007JE002997.
Zhou, L. et al., 2010. Cosmic-ray-mediated formation of benzene on the surface of Saturn's Moon Titan. Astrophys. J. 718, 1243–1251. http://dx.doi.org/10.1088/0004-637X/718/2/1243.